Petroleum and Coal

Article Open Access

Mineralogy, Provenance, Diagenesis and Reservoir Quality of the Sandstones from the Southern Bredasdorp Basin, Offshore South Africa

Temitope Love Baiyegunhi, Oswald Gwavava and Kuiwu Liu

Department of Geology, Faculty of Science and Agriculture, University of Fort Hare, Private Bag X1314, Alice, 5700, Eastern Cape Province, South Africa

Received December 5, 2022; Accepted May 26, 2023

Abstract

The Bredasdorp Basin covers the greater part of the larger Outeniqua Basin, representing a productive petroleum-bearing basin off the south coast of South Africa. However, uncertainty about the diagenesis, provenance, and their impacts on reservoir qualities of the sandstones has hindered further exploration, particularly in the southern Bredasdorp Basin. In this part of the basin, sandstones from the primary and secondary hydrocarbon targeted intervals within the 6At1 and 14At1 stratigraphic sequence were investigated using a combination of petrographic, mineralogical, and geochemical techniques. Petrographic studies show that the sandstones are largely subarkose. The provenance analysis indicates that the sandstones are largely derived from granites and granite–gneisses of a continental block tectonic provenance, suggesting that the sandstones were derived from stable shields and uplifted areas. Furthermore, the tectonic diagram suggests that the basin developed on a rift passive setting (trailing edge) of the stable continental margins. The main diagenetic processes that have affected the reservoir quality of the sandstones are cementation by authigenic clay, carbonate, and silica, growth of authigenic glauconite, dissolution of minerals and load compaction. The development of secondary porosity as a result of the partial to complete dissolution of calcite cement and some detrital grains (i.e., feldspar) has improved the reservoir quality of the sandstones. The scattered plots of porosity and permeability versus cement+clays show inverse correlations, signifying that the reservoir quality is mainly controlled by cementation and authigenic clays. In general, there is no particular diagenetic process that exclusively controls the type or form of porosity evolution in the sandstones.

Keywords: *Mineralogy; Provenance; Diagenesis; Reservoir quality; Sandstones; Bredasdorp Basin.*

1. Introduction

Early exploration for hydrocarbon reservoirs was originally focused on gaining knowledge on the regional tectonic setting of the host basin, followed by thorough assessment of local geology and stratigraphy [1]. Nonetheless, recent research findings indicate that the search for reservoir properties in sandstone requires a greater emphasis on diagenesis [2-3]. One of the major constraints on prospectivity during petroleum exploration is reservoir quality [4]. In petroleum exploration, remote sensing and geophysical methods are used to determine the presence of sandstones. They do not, however, provide any information or assistance in locating sandstones with high porosity and permeability that have been preserved due to diagenetic alteration [2]. As a result, it is critical to have a thorough understanding of the factors controlling reservoir quality in order to aid in the evaluation of the economic feasibility of petroleum discoveries. Once petroleum has been discovered in a basin, it is critical to have a thorough understanding of the diagenetic characteristics and evolution of the reservoir rock in order to predict its quality as a hydrocarbon reservoir and to aid in future exploration and appraisal efforts [5].

The reservoir quality of fine-grained clastic rocks is affected by a variety of interrelated factors such as pore water chemistry, mineral composition, temperature, diagenetic events, subsurface pressure, burial depth and time of uplift, depositional environment, and tectonic setting [2-3]. Several researchers, including [3,6-8], have reported that diagenetic changes or modifications in clastic rocks have a large impact on reservoir quality by modifying their original porosity and permeability, which in turns affects the reservoir quality. Petrography is an important tool for investigating the types and timing of diagenetic processes that affect the porosity and permeability of clastic rocks [9]. Furthermore, the economic importance of certain sandstone units as a source or reservoir rock for petroleum is determined by the units' diagenetic history as well as their original depositional characteristics [7,10]. Many studies have drawn these conclusions in the past [3,8,11-13], and many of the reactions and diagenetic alterations presented in these studies in particular are quite well understood.

Provenance studies of clastic sedimentary rocks frequently seek to reveal the composition and geological evolution of the sediment source areas, as well as to constrain the depositional basin's tectonic setting. Previous studies have shown that the chemical composition of clastic sediments is determined by a complex interplay of several variables, such as the composition of the source rock, the extent of weathering, transportation, and diagenesis [14-15]. However, the tectonic setting of the sedimentary basin may be more important than other factors, because different tectonic settings can provide different types of source materials with variable chemical signatures [16-18]. Many attempts have been made to improve provenance models using framework composition [19-21] and geochemical features [17,22-25].

The Bredasdorp Basin covers the greater part of the larger Outeniqua Basin, representing a productive petroleum bearing basin, off the south coast of South Africa (Figure 1) [26]. Due to the basin's hydrocarbon potential, a significant amount of research has been focused on its geology and petrophysical characterization over the last decade. Burden [1], Brown [27], Jungslager [28], McMillan [29], PASA [30-31], Broad [32], Tinker [33], and Akinlua [4] all made significant contributions to our understanding of the regional geology, petroleum prospects, and tectonic evolution of the Bredasdorp Basin, particularly in the northern and central parts. However, diagenetic changes in reservoir properties in the Bredasdorp Basin have yet to be reported or documented. In this regard, there is still a knowledge gap between reservoir properties and the factors influencing reservoir quality of Bredasdorp Basin sandstones. With the primary goal of closing the gap, this paper describes the tectonic provenance as well as how diagenesis and detrital composition influence the reservoir quality.

2. Geological setting

The Bredasdorp Basin is a south-easterly trending rift basin with half-graben structures. The Upper Jurassic, Lower Cretaceous, Cretaceous, and Cenozoic rift to drift strata dominate these half-grabens [27]. The basin formed, along with other sub-basins of the larger Outeniqua Basin, as a result of rift and drift activity along the Agulhas-Falkland Fracture Zone during the break-up of the Gondwana supercontinent [31]; (Figure 1). The Bredasdorp Basin, located off the south coast of South Africa (southeast of Cape Town and west-southwest of Port Elizabeth), is composed primarily of sandstones with subordinate mudrocks. The basin is approximately 80 km wide and 20 km long [32], with the western and eastern sides bounded by the Columbine-Agulhas Arch (CAA) and the Infanta Arch (IA), respectively [27]. The CAA and IA are extended basement highs composed of Cape Supergroup granite and Precambrian (basement) metamorphic rocks.

The Bredasdorp Basin was reported to have formed beneath the Indian Ocean along the South African continental margin during the initial stage of rifting in the late Jurassic-early Cretaceous [34]. According to Akinlua [4], the basin experienced a series of structural distortions during the break-up of Gondwanaland and the continents of the southern hemisphere. According to Tinker [33], the Falkland-Agulhas Fracture Zone (AFFZ) produced dextral transtensional stress or right-lateral shear movement as a result of the separation of the Falkland Plateau from the Mozambique Ridge as well as the break-up of west Gondwana. Normal faulting developed north of the AFFZ as a result of the tectonic events, resulting in the formation of graben and half-graben sub-basins (e.g., the Bredasdorp Basin) [27]. The basin is mostly filled with late Jurassic and early Cretaceous syn-rift continental and marine sediments, as well as post-Cretaceous and Cenozoic divergent rocks with slanting or inclined half-graben structures.

The basin is made up of an Oxfordian-Recent stratigraphic column [27,31] that overlies the Cape Supergroup [29]. The stratigraphic column depicts the occurrence of a syn-rift phase and a post-rift or drift phase [28]. The syn-rift phase is divided into two sedimentation phases: syn-rift I and syn-rift II [28]. The syn-rift I sedimentation occurred from the middle Jurassic to the late Valanginian (Basement to 1At1), whereas the syn-rift II sedimentation occurred from the late Valanginian to the Hauterivian (1At1 to 6At1) [31]; (Figure 2).

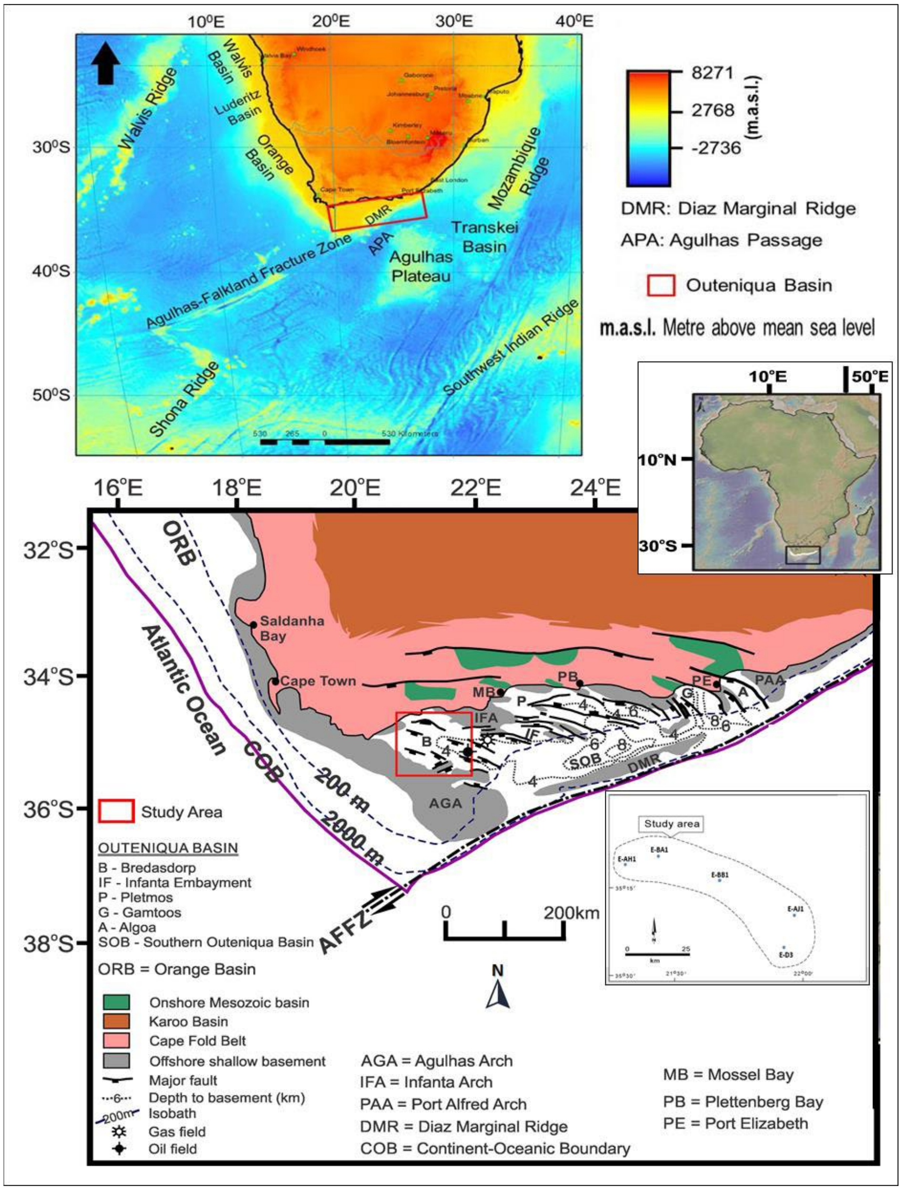

Figure 1. Geological map showing the Bredasdorp Basin and other South African southern offshore sedimentary basins [26]

The syn-rift I succession is terminated by a regional 1At1 unconformity, indicating the start of a renewed rifting (synrift II) phase caused by early movement along the AFFZ around 121 Ma (Valanginian-Hauterivian boundary) [28]. Later, during the Hauterivian-Early Aptian (6At1 to 13At1) period, the Transitional (Early Drift) phase occurred (Figure 2). The Transitional (Early Drift) phase was marked by recurring episodes of progradation and aggradation, and it was primarily influenced by tectonic events and eustatic sea-level changes [32]. This phase was considered the first deep water deposits in the Bredasdorp Basin, and they were deposited as a result of major subsidence of the basin as well as an increase in water depth. The late drift phase, on the other hand, coincided with a major marine regression in the Bredasdorp Basin during the early Aptian. The 13At1 unconformity is the result of a major erosion caused by this regression event. The erosion period is followed by a marine transgression, which transports and deposits organic-rich claystone in the basin under anoxic conditions [29]. The 14At1 mid-Albian unconformity (Figure 2) marks the beginning of active thermally driven subsidence when the Columbine-Agulhas Arch was cleared by the trailing edge of the Falkland Plateau in the Late Albian [32].

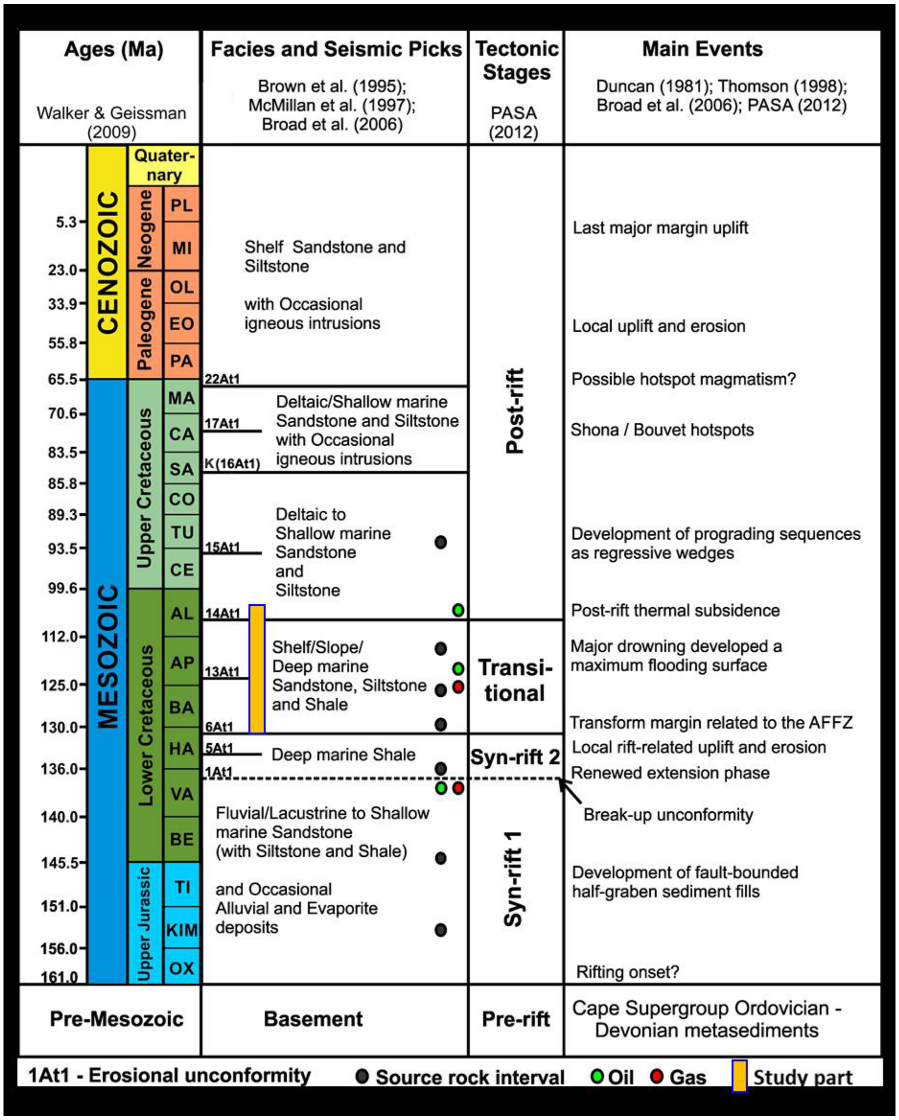

Figure 2 Stratigraphic chart of the Bredasdorp Basin showing main unconformities and tectonic stages with corresponding geodynamic events [26]

3. Materials and method

An optical microscope was used to examine 150 thin sections of 92 representative sandstone samples collected from exploration wells E-AH1, E-AJ1, E-BA1, E-BB1, and E-D3 to determine their mineralogical compositions and diagenetic characteristics. In addition, 50 of the 92 sandstones were cleaned, glued onto a glass microscope slide, and gold coated with a Cressington Gold Coater 108 Gold/A machine. The coated samples were examined using a scanning electron microscopy (SEM) instrument (Model: JEOL JSM-6390LV) equipped with an energy dispersive x-ray microanalyser (EDX). The samples were imaged using backscattered electron imaging (BSE) and secondary electron imaging (SEI). For the modal composition analysis, at least 500 points were counted per thin section using the procedures recommended by [20,35]. Each thin section was analyzed using an Olympus BX51 microscope equipped with an Olympus DP72 digital camera in accordance with [20] traditional point-counting technique. The framework components of the sandstones were categorized into quartz (monocrystalline and polycrystalline), feldspar, lithic fragments, mica, cement and matrix. Furthermore, the framework parameters of the detrital modes in the sandstones were recalculated to 100%, and ternary Qt-F-L diagrams were plotted for classification and provenance determination. During the point counting process, the amount of pore space was also taken into account. The thin section visual porosity was calculated using petrographic point counting, and the results were statistically compared to the existing poroperm porosity and permeability values for the exploration wells under consideration. The poroperm instrument is a combined permeameter and porosimeter that is used to determine the porosity and permeability of plug-sized cores at ambient confining pressure. The porosity and permeability determined using the poroperm instruments are referred to as poroperm porosity and permeability in this context. These porosity and permeability values were provided by the Petroleum Agency of South Africa (extracted from Soekor's database) and were incorporated into this study. The results of the SEM and petrographic analyses were used to comment on the porosity and permeability values. Furthermore, the mineral compositions of 30 sandstone samples were determined using X-ray diffraction (XRD). The backloading preparation method was used for the XRD analysis. The diffractograms were obtained using a Malvern PANalytical Aeris diffractometer with a PIXcel detector and fixed slits with Fe-filtered Co-Kα radiation. The phases were identified using the X'Pert Highscore plus software (version 2.1, PANalytical, Malvern, United Kingdom), and the relative phase amounts (wt. %) were estimated using the Rietveld method [36]. The petrographic microscopy was done at the Petroleum Agency of South Africa in Cape Town, while the SEM and EDX analyses were done at the University of Fort Hare in South Africa. The XRD analysis was carried out at the XRD Analytical and Consulting South Africa.

4. Results

4.1. Texture and mineralogy

The sandstones are fine to medium-grained and moderately sorted to moderately well sorted (Figure 3). In particular, borehole E-AH1 is mostly composed of massive, well-sorted, fine-to-medium-grained glauconitic sandstone and claystone with minor siltstone interbeds. The sandstones in borehole E-AJ1 are generally massive, fine-to-medium-grained, and rich in glauconite. They are moderately well organized. The presence of stylolites, which appear as irregular, undulatory, and coarsely sutured horizontal features and, less frequently, as finely sutured vertical to sub-vertical fractures, is a distinguishing feature in borehole E-AJ1. Borehole E-BA1 is mostly made up of massive, moderately well-sorted fine-to-medium-grained glauconitic sandstone, with some claystone and siltstone. The sandstone is slightly porous and light brownish-grey in color, with very fine to medium subangular grains that are well-sorted. The sandstone in borehole E-BB1 is mostly well-sorted, fine-grained, lithic (quartzite clasts), glauconitic, slightly shelly, and carbonaceous. Sandstones in borehole E-D3 are massive, moderately sorted, medium grained, and slightly glauconitic. The roundness of the grains in the sandstones ranges from subangular to rounded, and the sphericity ranges from low to high (mostly low; oblong grains). Quartz, feldspar, lithic fragments, and glauconite are the framework minerals of the sandstones, while mica (biotite and muscovite), zircon, and rutile are the accessory minerals. The quartz grains are usually subangular to rounded in shape and constitute about 52.2-68.0% of the framework grains (Table 1). The quartz occurs as both monocrystalline quartz (Qm) and polycrystalline quartz (Qp) grains and often exhibits undulose and planar extinctions. Monocrystalline quartz (Qm) predominates, accounting for approximately 97.04% of the total quartz grains in the sandstones.

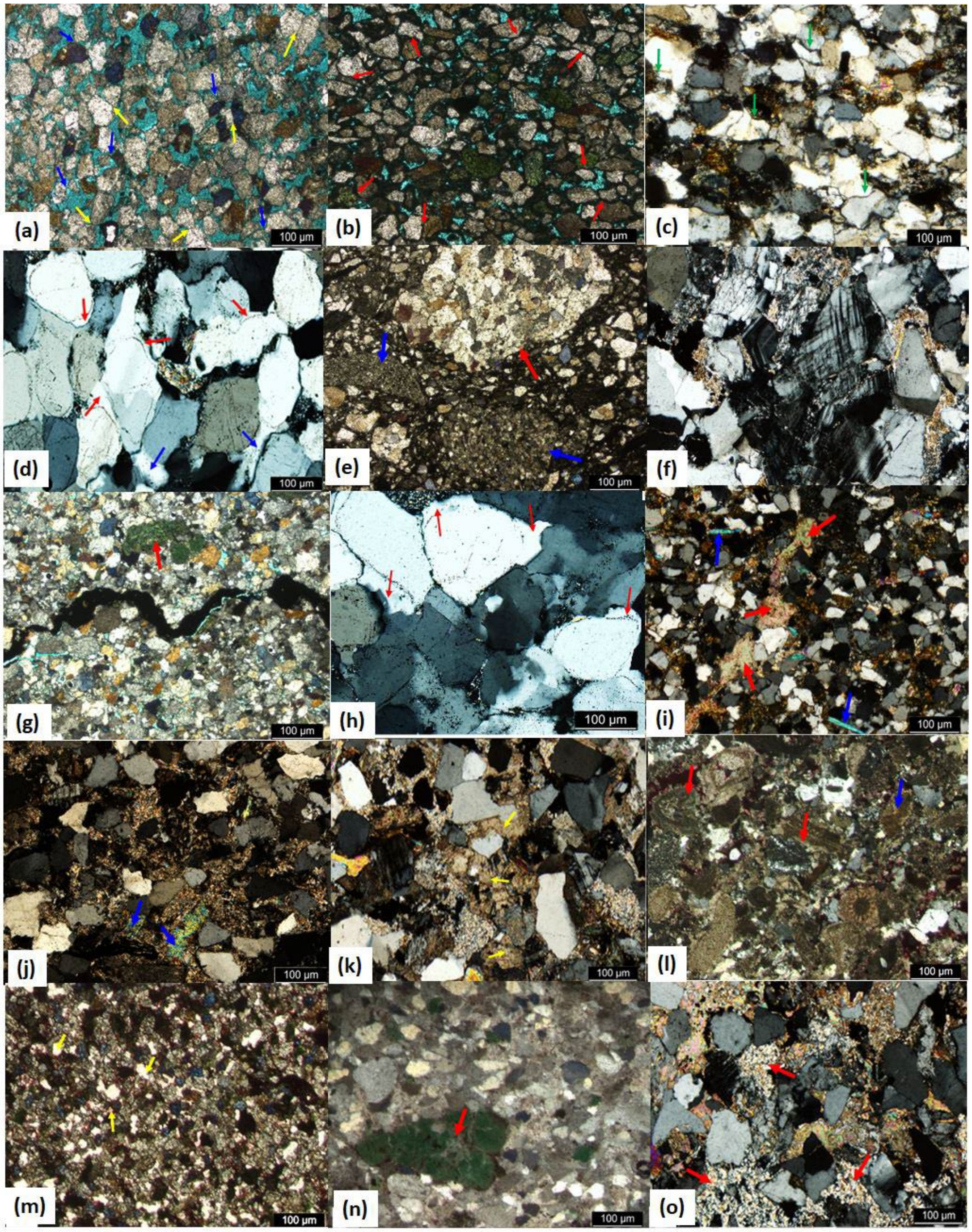

Figure 3. Thin section photomicrographs showing: (a-c) different grain to grain contact, point (blue arrows) and long (yellow arrows) contacts in borehole E-AH1, more compacted long contacts (red arrows) in borehole E-AJ1 and convano-convex (green arrows) in borehole E-BA 1; (d) authigenic quartz (blue arrows) and quartz overgrowths (red arrows) in borehole E-D3; (e) sedimentary lithic fragment (red arrow) and metamorphic lithic fragment (blue arrows); (f) albitization (bottom middle) of microcline (middle) in borehole E-AH1; (g) glauconite grain (red arrow); (h) authigenic or fine granular quartz cement (red arrows) in borehole E-AH1; (i) calcite cement (red arrows) and mica flakes (blue arrows) in borehole E-BB1; (j) mica (blue arrows) in clay matrix; (k) calcite cement (yellow arrows); (l) mud-pellets (blue arrow) and shell fragments (red arrows) in borehole E-D3; (m) ferroan calcite (yellow arrows) filling intergranular pores with chlorite component (brownish colour); (n) partial replacement of feldspar and matrix by glauconite (red arrows) in borehole E-AJ1; (o) Partial replacement of feldspar by clay minerals (red arrows).

Feldspar grains are frequently subangular to subrounded in shape and account for approximately 10.0-18.0% of the framework grains. Alkali feldspar (orthoclase and microcline) and plagioclase feldspar (albite) were observed, with orthoclase being the most dominant mineral. Quantitatively, only about 24% of the alkali feldspar (primarily orthoclase with a few microcline grains) appears to be twinned, whereas approximately 76% of the plagioclase appears to be untwinned. The lithic fragments account for approximately 5.0-10.2% of the framework grains, with an average of 7.8%. These lithic fragments are commonly found as fine quartz grains in clay matrix (sedimentary lithic fragment) and sutured grain clasts with no matrix (metamorphic lithic fragment). Sedimentary lithic fragments account for a greater proportion of total lithic fragments. The matrix accounts for about 3.2-13.8% of the total composition, while cement accounts for between 1.8 and 10.0%. The matrix is typically clay minerals and they are either detrital or formed diagenetically. The diagenetic matrix minerals are thought to have formed as a result of the alteration and precipitation of the framework grains, as well as the recrystallization of other matrix minerals. Similarly, XRD analysis reveals that the most abundant minerals are quartz (56.0-73.7%) and plagioclase (6.1-14.5%), with kaolinite (1.6-13.6%) being the dominant clay mineral (Table 2). Clay minerals observed in the sandstones include kaolinite, illite, smectite, and chlorite.

Table 1. Modal compositions of the studied sandstones from the Bredasdorp Basin

Borehole	Depth (m)	Qt (%)	Qm (%)	Qp (%)	F (%)	L (%)	GL (%)	Acc (%)	Cmt (%)	Mx (%)	QmFLt (%)			QtFL (%)		
											Qm	F	Lt	Qt	F	L
E-AH1	2471.0	59.0	57.6	1.4	13.4	7.4	4.2	0.2	3.8	12.0	72.2	16.8	11.0	73.9	16.8	9.3
	2473.0	52.2	52.0	0.2	13.0	9.2	4.4	1.0	6.4	13.8	69.9	17.5	12.6	70.2	17.5	12.4
	2475.0	58.8	56.0	2.8	14.2	5.8	5.0	0.3	6.4	9.5	71.1	18.0	10.9	74.6	18.0	7.4
	2478.0	56.2	53.8	2.4	13.6	5.2	4.0	0.4	7.0	13.6	71.7	18.1	10.1	74.9	18.1	6.9
	2479.0	68.0	65.8	2.2	10.8	7.4	3.8	0.1	5.6	4.3	76.3	12.5	11.1	78.9	12.5	8.6
	2481.0	62.4	59.6	2.8	12.4	5.4	2.6	0.2	4.6	12.4	74.3	15.5	10.2	77.8	15.5	6.7
	2482.0	65.2	62.2	3.0	10.0	6.4	3.0	0.1	5.0	10.3	76.2	12.3	11.5	79.9	12.3	7.8
	2483.0	65.8	63.8	2.0	14.2	5.2	5.0	1.0	5.6	3.2	74.9	16.7	8.5	77.2	16.7	6.1
E-AJ1	2701.3	66.2	64.2	2.0	13.8	6.6	4.2	0.3	4.2	4.7	74.1	15.9	9.9	76.4	15.9	7.6
	2702.5	68.4	66.6	1.8	14.2	5.6	1.0	0.1	6.4	4.3	75.5	16.1	8.4	77.6	16.1	6.3
	2703.0	61.0	59.0	2.0	14.0	5.0	4.0	0.8	6.4	8.8	73.8	17.5	8.8	76.3	17.5	6.3
	2704.0	52.2	51.8	0.4	15.2	6.2	4.0	0.4	8.6	13.4	70.4	20.7	9.0	70.9	20.7	8.4
	2705.0	59.8	59.6	0.2	18.8	6.2	3.0	0.4	4.2	7.6	70.3	22.2	7.5	70.5	22.2	7.3
	2721.0	60.4	60.2	0.2	19.8	5.8	3.0	0.2	3.0	7.8	70.0	23.0	7.0	70.2	23.0	6.7
	2722.0	66.0	65.4	0.6	15.2	7.8	2.2	0.2	1.8	6.8	73.5	17.1	9.4	74.2	17.1	8.8
	2724.0	60.2	59.8	0.4	10.6	5.6	3.6	0.8	9.4	9.8	78.3	13.9	7.9	78.8	13.9	7.3
	2726.0	60.6	59.2	1.4	13.6	7.2	2.4	0.5	5.8	9.9	72.7	16.7	10.6	74.4	16.7	8.8
	2728.0	62.0	61.0	1.0	17.6	5.8	3.2	0.6	3.8	7.0	71.4	20.6	8.0	72.6	20.6	6.8
	2730.0	61.0	60.4	0.6	15.2	9.6	1.4	0.1	5.8	6.9	70.4	17.7	11.9	71.1	17.7	11.2
	2970.0	60.0	59.0	1.0	15.0	8.4	3.0	0.4	4.6	8.6	70.7	18.0	11.3	71.9	18.0	10.1
	2973.0	61.4	60.0	1.4	13.8	9.4	3.0	0.2	4.2	8.0	70.9	16.3	12.8	72.6	16.3	11.1
	2975.0	60.2	58.8	1.4	10.0	8.2	5.0	0.0	10.0	6.6	75.0	12.8	12.2	76.8	12.8	10.5
	2977.0	60.0	59.8	0.2	15.0	10.0	5.0	0.0	5.0	5.0	70.4	17.6	12.0	70.6	17.6	11.8
	2979.0	60.4	59.6	0.8	14.2	5.6	0.4	0.2	7.6	11.6	74.3	17.7	8.0	75.3	17.7	7.0
	2982.0	60.0	59.8	0.2	15.0	10.0	3.2	0.1	5.0	6.7	70.4	17.6	12.0	70.6	17.6	11.8
	3037.0	60.2	59.6	0.6	14.4	5.2	2.2	1.0	5.0	12.0	74.7	18.0	7.3	75.4	18.0	6.5
	3039.0	62.0	61.2	0.8	12.0	5.2	3.8	0.4	5.8	10.8	77.3	15.2	7.6	78.3	15.2	6.6
	3041.0	65.0	64.0	1.0	10.4	9.6	3.0	0.8	4.2	7.0	75.3	12.2	12.5	76.5	12.2	11.3
	3043.0	64.4	63.8	0.6	10.0	9.6	3.2	1.0	5.2	6.6	76.0	11.9	12.1	76.7	11.9	11.4
	2692.0	64.0	63.8	0.2	10.6	10.2	5.0	0.4	4.4	5.4	75.2	12.5	12.3	75.5	12.5	12.0
	2695.0	65.6	64.4	1.2	14.6	9.8	2.6	0.6	3.2	3.6	71.6	16.2	12.2	72.9	16.2	10.9
	2698.0	64.6	63.8	0.8	16.6	5.4	5.6	0.6	3.8	3.4	73.7	19.2	7.2	74.6	19.2	6.2
	2701.0	64.0	63.6	0.4	14.0	9.0	5.0	0.0	3.0	5.0	73.1	16.1	10.8	73.6	16.1	10.3
	2705.0	64.2	63.2	1.0	14.4	10.2	2.8	0.6	2.8	5.0	71.2	16.2	12.6	72.3	16.2	11.5

Borehole	Depth (m)	Qt (%)	Qm (%)	Qp (%)	F (%)	L (%)	GL (%)	Acc (%)	Cmt (%)	Mx (%)	QmFLt (%)			QtFL (%)		
											Qm	F	Lt	Qt	F	L
	2708.0	61.2	60.0	1.2	14.8	9.2	5.0	1.0	3.8	5.0	70.4	17.4	12.2	71.8	17.4	10.8
E-BA1	2828.0	60.0	59.4	0.6	13.8	8.6	3.6	0.0	3.6	10.4	72.1	16.7	11.2	72.8	16.7	10.4
	2829.0	60.4	59.8	0.6	14.0	8.8	2.8	0.6	3.8	9.6	71.9	16.8	11.3	72.6	16.8	10.6
	2830.0	62.0	61.8	0.2	14.4	8.6	3.6	0.4	3.6	7.4	72.7	16.9	10.4	72.9	16.9	10.1
	2832.0	68.4	67.6	0.8	13.8	8.0	2.0	0.2	2.4	5.2	74.9	15.3	9.8	75.8	15.3	8.9
	2834.0	64.6	64.4	0.2	13.4	6.4	2.8	0.2	3.8	8.8	76.3	15.9	7.8	76.5	15.9	7.6
	2836.0	63.2	62.8	0.4	14.6	7.2	3.6	0.6	3.6	7.2	73.9	17.2	8.9	74.4	17.2	8.5
	2838.0	64.6	64.0	0.6	14.0	5.8	2.4	0.4	5.0	7.8	75.8	16.6	7.6	76.5	16.6	6.9
	2839.0	59.8	58.4	1.4	14.2	7.6	2.0	0.6	4.4	11.4	71.6	17.4	11.0	73.3	17.4	9.3
	2842.0	59.6	59.4	0.2	13.8	7.0	3.4	0.2	6.0	10.0	73.9	17.2	9.0	74.1	17.2	8.7
	2843.0	55.6	54.6	1.0	14.4	7.4	3.0	0.4	7.0	12.2	70.5	18.6	10.9	71.8	18.6	9.6
	2850.0	64.2	63.8	0.4	18.6	6.0	2.2	0.0	2.2	6.8	71.8	20.9	7.2	72.3	20.9	6.8
E-BB1	2537.2	60.4	60.0	0.4	13.0	6.2	2.6	0.0	4.0	13.8	75.4	16.3	8.3	75.9	16.3	7.8
	2537.7	62.0	61.8	0.2	14.0	6.0	2.0	0.2	6.2	9.6	75.4	17.1	7.6	75.6	17.1	7.3
	2539.0	55.6	54.2	1.4	14.0	6.2	4.2	0.2	6.8	13.0	71.5	18.5	10.0	73.4	18.5	8.2
	2541.0	68.2	67.2	1.0	16.4	5.8	1.8	0.4	2.2	5.2	74.3	18.1	7.5	75.4	18.1	6.4
	2543.0	66.0	65.8	0.2	13.2	6.2	2.2	0.6	2.6	9.2	77.0	15.5	7.5	77.3	15.5	7.3
	2546.0	65.0	64.4	0.6	15.8	6.8	2.0	0.0	2.4	8.0	73.5	18.0	8.4	74.2	18.0	7.8
	2548.0	62.2	60.4	1.8	15.2	6.8	4.2	0.4	3.6	7.6	71.7	18.1	10.2	73.9	18.1	8.1
	2551.0	60.0	59.8	0.2	13.8	6.4	4.0	0.4	3.6	11.8	74.6	17.2	8.2	74.8	17.2	8.0
	2553.0	57.8	57.4	0.4	13.6	6.0	3.6	0.3	7.0	11.7	74.2	17.6	8.3	74.7	17.6	7.8
	2556.0	61.6	60.8	0.8	13.0	5.0	2.2	0.6	5.2	12.4	76.4	16.3	7.3	77.4	16.3	6.3
	2659.0	62.0	60.6	1.4	15.6	6.0	2.4	0.8	3.6	9.6	72.5	18.7	8.9	74.2	18.7	7.2
	2660.0	60.2	59.6	0.6	14.4	7.2	3.2	0.6	4.2	10.2	72.9	17.6	9.5	73.6	17.6	8.8
	2662.0	61.2	60.0	1.2	14.0	8.2	2.6	0.4	3.6	10.0	71.9	16.8	11.3	73.4	16.8	9.8
	2663.0	61.6	60.8	0.8	16.4	7.8	2.4	0.6	3.2	8.0	70.9	19.1	10.0	71.8	19.1	9.1
	2665.0	63.2	62.2	1.0	13.6	7.4	3.6	0.0	3.8	8.4	73.9	16.2	10.0	75.1	16.2	8.8
	2719.0	64.0	63.8	0.2	14.0	5.2	3.2	0.2	4.2	9.2	76.7	16.8	6.5	76.9	16.8	6.3
	2721.0	60.2	60.0	0.2	15.0	6.6	3.0	0.6	4.6	10.0	73.3	18.3	8.3	73.6	18.3	8.1
	2723.0	57.6	56.6	1.0	14.8	6.8	4.2	0.0	5.6	11.0	71.5	18.7	9.8	72.7	18.7	8.6
	2847.0	59.0	58.8	0.2	16.8	6.0	2.0	0.4	5.0	10.8	71.9	20.5	7.6	72.1	20.5	7.3
	2849.0	61.4	60.4	1.0	13.8	7.6	2.4	0.2	5.0	9.6	72.9	16.7	10.4	74.2	16.7	9.2
	2851.0	61.8	61.4	0.4	14.2	6.0	1.8	0.6	4.8	10.8	74.9	17.3	7.8	75.4	17.3	7.3
	2853.0	60.0	59.0	1.0	11.0	5.2	3.0	0.8	8.0	12.0	77.4	14.4	8.1	78.7	14.4	6.8
	2855.0	61.0	60.6	0.4	14.0	5.8	1.4	0.2	5.8	11.8	75.0	17.3	7.7	75.5	17.3	7.2
	2858.0	58.0	57.2	0.8	12.6	6.6	3.0	0.6	7.0	12.2	74.1	16.3	9.6	75.1	16.3	8.5
	2860.0	60.2	59.4	0.8	13.6	7.0	2.0	0.2	5.0	12.0	73.5	16.8	9.7	74.5	16.8	8.7
	2863.0	55.4	55.2	0.2	16.0	6.8	2.4	0.0	6.8	12.6	70.6	20.5	9.0	70.8	20.5	8.7
	2865.0	57.0	56.6	0.4	13.0	6.0	2.4	0.4	8.4	12.8	74.5	17.1	8.4	75.0	17.1	7.9
	2872.0	57.2	57.0	0.2	15.2	7.0	2.2	0.1	6.0	12.3	71.8	19.1	9.1	72.0	19.1	8.8
	2872.8	59.2	59.0	0.2	14.0	5.4	4.2	0.2	5.0	13.0	75.1	17.8	7.1	75.3	17.8	6.9
	2873.0	57.6	56.2	1.4	13.6	5.6	3.0	0.1	7.2	12.9	73.2	17.7	9.1	75.0	17.7	7.3
	2873.8	56.0	55.6	0.4	15.6	7.8	4.0	0.4	6.6	9.6	70.0	19.6	10.3	70.5	19.6	9.8
	3280.4	59.8	59.6	0.2	17.6	8.0	1.8	0.6	4.2	8.0	69.8	20.6	9.6	70.0	20.6	9.4
	3282.0	59.2	59.0	0.2	18.0	8.2	3.0	0.0	2.0	9.6	69.1	21.1	9.8	69.3	21.1	9.6
	3284.0	57.6	57.4	0.2	12.4	7.2	2.0	0.2	9.0	11.6	74.4	16.1	9.6	74.6	16.1	9.3
	3286.0	60.0	59.8	0.2	13.6	9.0	1.8	0.2	6.0	9.4	72.4	16.5	11.1	72.6	16.5	10.9
	3288.0	59.0	58.4	0.6	14.0	6.0	3.8	0.0	6.2	11.0	73.9	17.7	8.4	74.7	17.7	7.6
	3292.7	59.8	59.4	0.4	16.2	7.2	2.6	0.0	5.6	8.6	71.4	19.5	9.1	71.9	19.5	8.7
	3294.0	58.0	57.0	1.0	13.6	7.8	1.6	0.0	7.0	12.0	71.8	17.1	11.1	73.0	17.1	9.8
E-D3	3261.2	62.4	62.2	0.2	13.4	7.2	1.6	0.2	4.4	10.8	74.9	16.1	8.9	75.2	16.1	8.7
	3262.9	61.8	60.4	1.4	16.8	5.8	2.8	0.6	3.8	8.4	71.6	19.9	8.5	73.2	19.9	6.9
	3266.5	60.0	58.6	1.4	12.4	6.0	3.8	0.2	7.8	9.8	74.7	15.8	9.4	76.5	15.8	7.7

Borehole	Depth (m)	Qt (%)	Qm (%)	Qp (%)	F (%)	L (%)	GL (%)	Acc (%)	Cmt (%)	Mx (%)	QmFLt (%)			QtFL (%)		
											Qm	F	Lt	Qt	F	L
	3268.0	63.0	62.2	0.8	15.0	6.4	2.4	0.8	4.4	8.0	73.7	17.8	8.5	74.6	17.8	7.6
	3269.0	58.4	58.0	0.4	14.4	6.8	3.6	0.0	5.0	11.8	72.9	18.1	9.0	73.4	18.1	8.5
	3526.0	62.0	60.8	1.2	14.0	6.2	3.2	0.2	5.4	9.0	74.0	17.0	9.0	75.4	17.0	7.5
	3528.5	59.2	58.2	1.0	13.4	5.2	2.2	0.0	6.2	13.8	74.8	17.2	8.0	76.1	17.2	6.7
	3529.5	62.8	62.2	0.6	15.6	6.2	2.6	0.1	4.2	8.5	73.5	18.4	8.0	74.2	18.4	7.3

Note: Qt= total quartz (Qm + Qp), Qm = monocrystalline quartz, Qp = Ploycrystalline quartz, F = Feldspar, L = Unstable siliciclastic lithic fragments (Lv + Ls + Lm), Ls = Sedimentary lithic fragment, Lv = Volcanic plus igneous lithic fragment, Lm = Metamorphic lithic fragment, Lt = Total siliclastic lithic fragment (L + Qp), GL = Glauconite, Acc = Accessory minerals, cmt = Cement, Mx = Matrix

Table 2. Mineralogical composition of the studied sandstone samples from XRD.

	Depth (m)	Quartz (%)	Pyrite (%)	Muscovite (%)	Kaolinite (%)	Plagioclase (%)	Glauconite (%)	Rutile (%)	Dolomite (%)	Calcite/ (%)	Chlorite (%)	Microcline (%)	Smectite (%)	Illite (%)
E-AH1	2471	56.1	2.1	5.8	13.6	6.1	4.1	0.0	0.4	9.4	0.1	1.3	0.6	0.5
	2475	67.6	0.9	1.2	4.1	7.3	1.7	0.0	0.3	12.8	0.6	1.6	0.0	1.6
	2478	69.4	1.0	0.9	7.4	8.9	0.6	0.1	0.1	6.4	0.3	4.5	0.1	0.0
	2481	68.2	0.4	3.5	3.9	9.2	1.8	0.2	0.3	7.9	0.6	3.7	0.1	0.0
	2483	67.4	0.3	2.2	5.3	9.7	2.0	0.0	0.2	9.4	0.4	2.1	0.3	0.5
E-AJ1	2703	73.7	0.2	1.1	4.0	8.3	0.1	0.1	0.6	9.0	0.3	2.1	0.1	0.3
	2721	68.5	0.2	1.2	5.0	9.2	1.9	0.1	0.7	10.4	0.8	1.7	0.0	0.2
	2726	69.4	0.3	1.0	1.6	10.2	0.6	0.5	2.4	10.9	1.3	1.3	0.0	0.4
	2730	63.5	0.1	5.6	10.4	11.1	0.2	0.4	0.2	7.1	0.2	1.1	0.1	0.0
	2970	71.5	0.2	5.9	3.7	12.8	1.3	0.1	0.0	3.0	0.3	0.8	0.2	0.3
	2982	69.7	0.6	4.7	6.6	14.5	0.6	0.3	0.2	1.8	0.1	0.4	0.2	0.2
	3039	68.4	0.4	3.2	5.1	12.1	0.9	0.6	0.3	5.4	1.0	2.1	0.1	0.3
E-BA1	2828	63.7	5.9	1.5	4.2	10.1	0.3	0.2	1.8	7.1	2.7	1.6	0.1	0.8
	2832	68.7	0.3	2.2	3.7	14.5	0.2	0.1	0.1	8.1	0.5	1.4	0.0	0.0
	2838	69.4	0.2	1.7	7.1	8.5	0.4	0.2	0.1	10.2	0.1	1.6	0.2	0.0
	2843	61.9	0.7	2.0	6.8	9.3	0.3	0.3	0.0	16.8	0.3	1.3	0.2	0.1
	2850	61.7	0.7	1.8	5.3	13.4	1.7	0.1	0.2	12.9	0.3	1.0	0.1	0.5
E-BB1	2539	60.7	4.4	13.3	6.2	10.6	0.6	0.3	0.0	0.4	2.8	0.7	0.0	0.0
	2548	60.1	2.5	2.6	6.9	9.8	0.1	0.1	0.0	13.5	1.2	2.8	0.1	0.1
	2556	71.4	1.7	4.1	4.6	10.3	0.7	0.1	0.1	5.0	0.9	0.8	0.0	0.0
	2662	70.4	1.9	4.2	4.7	9.6	0.3	0.19	0.2	4.2	1.0	3.2	0.0	0.0
	2721	63.9	0.9	2.8	6.2	14.7	0.2	0.2	0.0	7.7	1.4	1.2	0.1	0.5
	2849	67.6	0.2	2.1	4.9	15.2	0.1	0.0	0.1	6.9	0.8	1.4	0.0	0.7
	2863	65.2	0.8	2.0	7.8	13.0	0.7	0.0	0.1	8.0	0.7	1.0	0.1	0.4
	3284	70.0	0.3	1.4	5.2	8.9	0.4	0.0	0.2	11.7	0.4	1.0	0.0	0.2
	3294	67.4	0.5	3.0	6.0	11.8	0.5	0.6	0.5	8.2	0.8	0.5	0.0	0.0
E-D3	3261	68.4	1.0	2.5	5.1	10.6	0.4	0.5	0.6	7.1	0.7	2.6	0.1	0.2
	3269	65.3	0.20	6.6	7.1	9.5	0.5	0.5	0.3	5.3	2.1	1.0	0.0	0.2
	3526	67.5	0.3	3.4	6.0	12.3	1.1	0.3	0.2	4.3	1.6	2.4	0.0	0.4
	3529	70.8	0.2	2.8	5.4	11.0	1.3	0.2	0.1	6.2	0.4	0.9	0.3	0.4

4.2. Diagenesis of sandstones

The primary diagenetic processes that have affected the sandstones are cementation and compaction, as well as the dissolution, replacement, and recrystallization of minerals. Cementation is the diagenetic process whereby authigenic minerals grow or precipitate around grains and in the pore spaces of sediments, which binds the detrital grains together. The cements that bind the framework grains of the sandstones are mainly carbonate (calcite), silica (quartz), glauconite, sulfide (pyrite), chlorite, and authigenic clay cements. The observed carbonate cement in the sandstones is calcite cement. This cement precipitates in the intergranular pores and is often seen to have replaced detrital quartz and feldspar. Calcite cement occurs as ferroan and non-ferroan calcite (Figure 4a), with the non-ferroan calcite being the most dominant type of carbonate cement. The ferroan calcite cement is observed as scattered patchy crystals and as isolated pore fillings. Occasionally, the ferroan calcite cement fills both the primary and secondary intergranular pores. On the other hand, the non-ferroan calcite cements occur as poikilotopic pore-filling crystals, which generally fill in the primary pores and replace feldspar and quartz grains. Silica cement occurs in the sandstones as authigenic quartz in pore spaces and as euhedral syntaxial form around quartz grains as overgrowths (Figure 4d). Glauconite cement is another common cement type in the sandstones and it is visible as a greenish colour (Figure 3g, 3n). It directly precipitates in the intergranular pore space, lines on the grain surfaces and fractures or cracks. Quantitatively, the glauconite cement ranges from about 0.4-3.6%, averaging 2.1% of the overall composition. The initial process of glauconitization of the detrital K-feldspars is seen in the form of small blebs along the grain boundaries, cleavage planes, and fractures until the feldspar is completely replaced.

Clay minerals or matrix are the most common cementing materials in the Bredasdorp Basin sandstones, occurring as pore lining and pore-filling cement (Figures 3k, 3o, 4a). The observed authigenic clay minerals in the sandstones are kaolinite, illite, and smectite. These clay minerals are formed as a result of recrystallization of fine matrix and dissolution of K-feldspars. Alternatively, the clay minerals could have been formed due to the alteration of one kind of clay mineral to another (i.e., the transformation of smectite and kaolinite into illite). Kaolinite in the sandstone is observed under SEM as fibrous or booklets and vermicular aggregates in the mud matrix and mud intraclast, occurring as pore filling and pore lining cement (Figure 4g). This kaolinite is also observed occurring as a replacement mineral, replacing some of the detrital K-feldspar and muscovite grains. Illite is observed under SEM as fabric-like and lath-like crystals or vermicular aggregates within mud intraclast and mud matrix. Illite is found as pore filling and pore lining in cement, as well as as vermicular stacked platelets within kaolinite that are oriented perpendicular to grain surfaces (Figure 4j). Occassionally, illites are seen growing from the surfaces of the curved flake smectite, forming a mixed illite-smectite interlayer (Figure 4m). SEM observation revealed that smectite in the sandstone generally has honey-comb and curved flake (cornflake-shaped texture) shapes (Figure 4n).

The observed smectite occurs as microcrystalline matrix aggregates and as grain lining or coating cement. Also, smectite flakes recrystallized into pelletic and fibrous illite through the process of illitization. The pyrite (FeS_2) cement is the least frequent cement type in the sandstones, and when present, it is seen in the form of framboidal and poikilotopic pyrite cements (Figure 4q). The poikilotopic pyrite cements are very large crystalline pyrites that fill secondary pore spaces and are often subhedral in shape. SEM observation has shown that the framboidal pyrites are densely packed with spherical aggregates of submicron-sized pyrite crystals (Figure 4q). These framboidal pyrites are observed occurring in the pore spaces between grains and coats or the surrounding grains. Petrographic and SEM studies revealed kaolinitization and illitization of weak detrital K-feldspar. Occassionally, muscovite grains are partially replaced by clay minerals, particularly along the boundaries (Figure 3j). SEM observation shows that dissolved K-feldspars are partially to completely replaced by diagenetic clay minerals, especially kaolinite. In places where the replacement is partial or minor, the original feldspar grain outline is still seen or preserved. In such feldspars, kaolinite commonly appears as arrays consisting of several, parallely arranged and densely packed crystals that attack or penetrate the edges as well as the surface of the feldspar grain. Consequently, relics of feldspars are usually present within the matrix of the kaolinite crystals. Alternatively, in places where the replacement is major or extensive, the kaolinite occurs as numerous stacked-like crystals and separate booklets that achieve relatively high intercrystalline porosity and severely penetrate the surface of the feldspar grain.

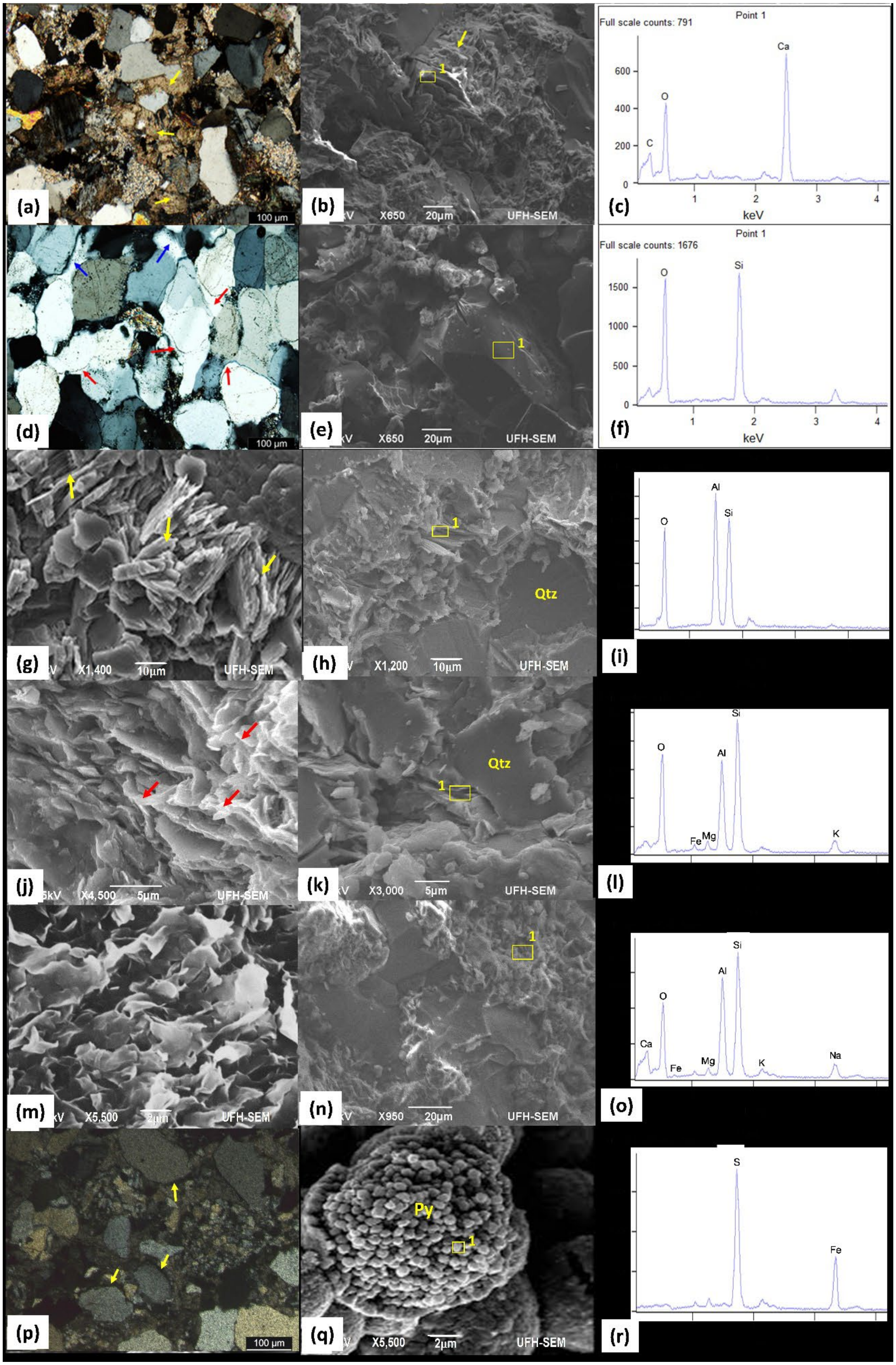
(a)
100 µm
(b)
X650
20µm
UFH-SEM
(c)
Full scale counts: 791
Point 1
Ca
O
C
keV
(d)
100 µm
(e)
X650
20µm
UFH-SEM
(f)
Full scale counts: 1676
Point 1
O
Si
keV
(g)
X1,400
10µm
UFH-SEM
(h)
X1,200
10µm
UFH-SEM
Qtz
(i)
Al
Si
O
(j)
X4,500
5µm
UFH-SEM
(k)
X3,000
5µm
UFH-SEM
Qtz
(l)
Si
O
Al
Fe
Mg
K
(m)
X5,500
UFH-SEM
(n)
X950
20µm
UFH-SEM
(o)
Si
Al
O
Ca
Fe
Mg
K
Na
(p)
100 µm
(q)
Py
X5,500
2µm
UFH-SEM
(r)
S
Fe

Figure 4. (a) Photomicrograph showing calcite cement (yellow arrows); (b) SEM (BSE) image of regular rhombohedron calcite (yellow arrow) with irregular clevaged calcite; (c) EDX spectrum showing elemental compositions of calcite at point 1 in Figure 4b; (d) Thin section photomicrograph of sandstone from Borehole E-D3 showing authigenic quartz cement (blue arrows) and quartz overgrowths (red arrows); (e) SEM (BSE) image of euhedral quartz crystal (left side) with pyramid-like surfaces in sandstone from Borehole E-D3; (f) EDX spectrum showing elemental composition of quartz at point 1 in Figure 4e; (g) SEM (BSE) photomicrograph showing aggregates of booklet-like kaolinite (yellow arrows) in sandstone from Borehole E-AH1; (h) SEM (BSE) image showing accordion or booklet-shaped kaolinite (yellow box), and quartz grain; (i) EDX spectrum showing elemental compositions of kaolinite at point 1 in Figure 4h; (j) SEM (BSE) image showing authigenic illite with incipient lath-like or fibrous forms growing from original smectite; (k) SEM (BSE) photomicrograph showing rod/fibrous shape illite (yellow box) and quartz grain; (l) EDX spectrum showing elemental compositions of illite at point 1 in Figure 4k; (m) SEM (BSE) photomicrograph showing mixed smectite-illite laye; (n) SEM (BSE) photomicrograph showing honey-comb shaped smectite (yellow box); (o) EDX spectrum showing elemental compositions of smectite at point 1 in Figure 4n; (p) Photomicrograph showing authigenic pyrite cement in the form of thin rim or patch surrounding framework grains; (q) SEM (BSE) photomicrograph of authigenic framboid pyrite; (r) EDX spectrum showing elemental composition of pyrite at point 1 in Figure 4q

5. Interpretations and discussion

5.1. Classification of sandstones

The most widely used and effective methods for classifying sandstones combine the textural criteria (i.e. proportion of the matrix) with the compositional criteria (i.e. percentages of the framework grains) [16,20,37-38]. In this study, the classification of the sandstones is based on the QFL (quartz, feldspar, and lithic fragments) classification schemes proposed by [37-38], as well as the geochemical classification diagrams of [16,39]. The classification methods of [37-38] show that the sandstones could be classified as subarkosic wacke (Figure 5a-b).

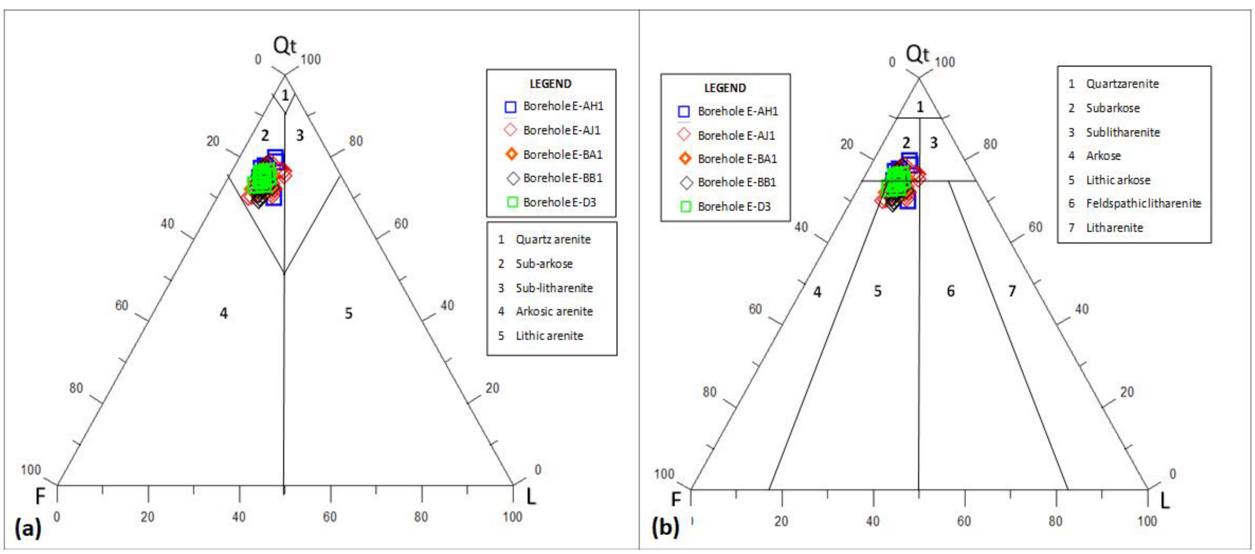

Figure 5. (a) Sandstone modal data plot of the total quartz-feldspar-lithic fragments (Qt-F-L) on the background ternary diagram of [37]; (b) Sandstone modal data plot of the total quartz-feldspar-lithic fragments (Qt-F-L) on the background ternary diagram of [38]

5.2. Provenance and tectonic setting

Several researchers, including Dickinson and Suczek [35] and Dickinson [20], Banerjee and Banerjee [40], Oghenekome [41] , Baiyegunhi [42], and Chima [43], have used the Qt-F-L ternary diagram to link detrital framework grains of sandstone to different provenance settings (i.e., stable cratons, basement uplifts, magmatic arcs, and recycled orogens). The studied sandstones were plotted on the background Qt-F-L ternary diagrams of [20,35,44-46] to interpret and discriminate between the various types of tectonic settings and provenances. In the Qt-

F-L ternary diagram of [35], the sandstones fall in the recycled orogen field (Figure 6a), indicating that the sandstones were primarily sourced from siliciclastic rocks with less volcanic rocks. As a result of orogenic uplifted fold-belts and thrust sheets, the rocks have been metamorphosed to some extent and are prone to erosion [20]. As evidenced in the modal composition, Dickinson [20] reported that sands sourced from recycled orogens typically have a low percentage of feldspar due to the fact that igneous rocks are not the primary sources. The ternary plot of Qt-F-L on the background provenance diagram of [45] revealed that the sandstones plot in the transitional continental and craton interior fields of the continental blocks (Figure 6b), implying that the sandstones were derived from stable shields and platforms or uplifted areas, which mark plate boundaries and patterns of intraplate deformation that divide the continental blocks.

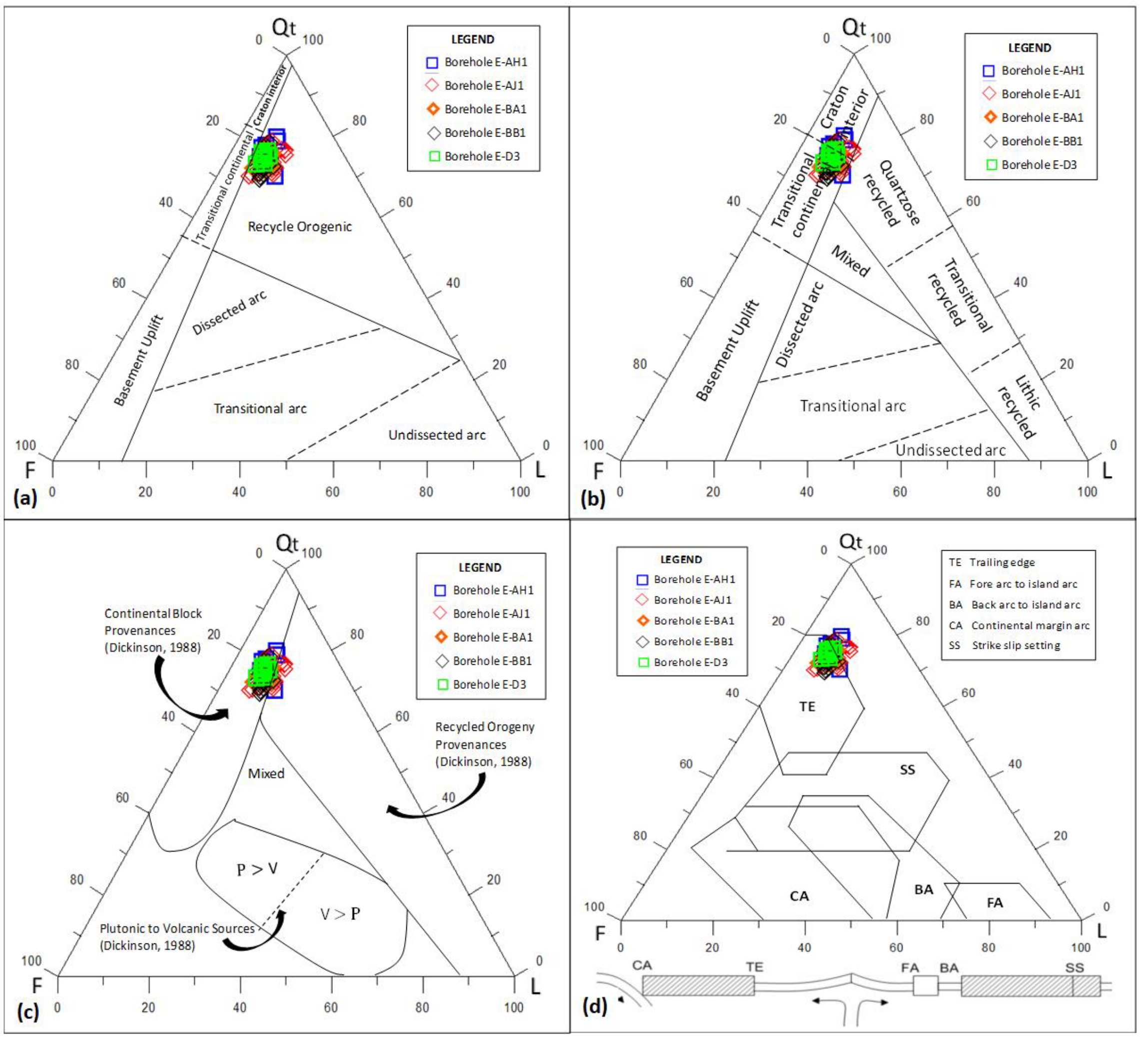

Figure 6. Total quartz-feldspar-lithic fragment (Qt-F-L) plot for framework modes of the sandstones on the background ternary diagram of [35] showing tectonic provenance; (b) Total quartz-feldspar-lithic fragment (Qt-F-L) plot for framework modes of the sandstones on the background diagram of [45] showing tectonic provenance; (c) Modal analysis data plot of the sandstones on the total quartz-feldspar-lithic fragment (Qt-F-L) ternary diagram of [45] showing tectonic provenance; (d) Total quartz-feldspar-lithic fragment (Qt-F-L) scheme proposed by [44] showing tectonic provenance of the sandstones

According to Dickinson [20], these basement uplifts are commonly found along incipient rift belts, transform ruptures, deep-seated thrusts, and wrench tectonic zones. Sandstones that are plotted in the craton field are matured sandstones and may have been sourced from relatively low-lying granitoid and gneissic sources, supplemented by recycled sands from associated platform or passive margin basins [20]. In the Qt-F-L ternary diagram of Dickinson [45], the sandstones are plotted in the fields of continental block and recycled orogenic provenances with stable craton sources and uplift in the basement complexes (Figure 6c). The modal analysis data plot of the sandstones on the Qt-F-L ternary diagram of [44] show that the sandstones are related to the trailing edge setting (Figure 6d), which is tectonically inactive and where the continental margin is facing a spreading center or rifting, resulting in the development of the Bredasdorp Basin on the trailing edge of the continent.

The sandstones are thought to be the trailing edge of the African plate, which separated from the South American plate millions of years ago and receded to form the Bredasdorp Basin. Large amounts of clay-sized materials and sand from the continents were deposited along the seaward side of the plates as their edges gradually contracted and subsided. The samples plotted outside of the tectonic setting fields are likely the result of intense weathering of the sandstones in the depositional basin. The petrographic and modal compositional analyses revealed that the sandstones have properties similar to those of the passive margin setting. According to McLennan [47], passive margin sandstones derived from plate interiors or stable continental margins typically have a high quartz content, which is also evident in the sandstones of the Bredasdorp Basin. In a regional context of the evolution of the Bredasdorp Basin, the results presented in this study are consistent with the assumption that during the Late Jurassic-Early Cretaceous break-up and separation of Gondwana, a large composite intracratonic rift basin was generated in the basin as a result of thermal subsidence in response to a single rifting event.

5.3. Reservoir properties

The main properties that determine the quality of a reservoir rock are the relationship and percentages of porosity and permeability. These properties play an important role in sandstone diagenesis by controlling the flow of fluids through them. The fluid that flows through the sandstone causes mineral dissolution, cementation, and authigenesis. Porosity and permeability are influenced to some extent by the textural characteristics such as grain size, shape, packing, and arrangement. The thin section visual porosity was calculated using petrographic point counting, and the results were statistically compared to the existing poroperm porosity and permeability values for the exploration wells under consideration. The poroperm instrument is a combined permeameter and porosimeter that is used to determine the porosity and permeability of plug-sized cores at ambient confining pressure. The porosity and permeability determined using the poroperm instrument are referred to as poroperm porosity and permeability. These porosity and permeability values were provided by the Petroleum Agency of South Africa (extracted from the Soekor's database) and were incorporated into this study. The results of SEM and petrographic analyses were used to comment on these porosity and permeability values. Intergranular (pore space between grains) and microporosity (matrix micropores) are the primary porosities in the sandstones, while secondary porosities are secondary intragranular, dissolution, and fractured pores (Figure 7).

The sandstones' point count porosity values range from 1.9% to 22.7%, with an average of 11.8%. (Table 3). Specifically, the point count porosity for exploration wells E-AH1, E-AJ1, E-BA1, E-BB1 and E-D3 is 11.4–22.7%, 9.4–17.2%, 22.4–13.9%, 3.7–15.3%, and 1.4–14.3%, respectively. The exploration well E-AH1 has the highest point count porosity and gas expansion porosity, while the exploration well E-AJ1 has the lowest. With regard to the exploration wells E-AH1, E-AJ1, E-BA1, E-BB1, and E-D3, the gas expansion porosity varies from 14.2 to 20.6%, 6.7 to 16.8%, 9.1 to 11%, 2.8 to 14.3%, and 1.5 to 16%, respectively. For the exploratory wells E-AH1, E-AJ1, E-BA1, E-BB1, and E-D3, the permeability values vary from 22 to 61 mD, 0.6 to 19.4 mD, 0.3 to 11.7 mD, 0.01-28.1 mD, and 0.01 to 7.9 mD, respectively (Figure 8).

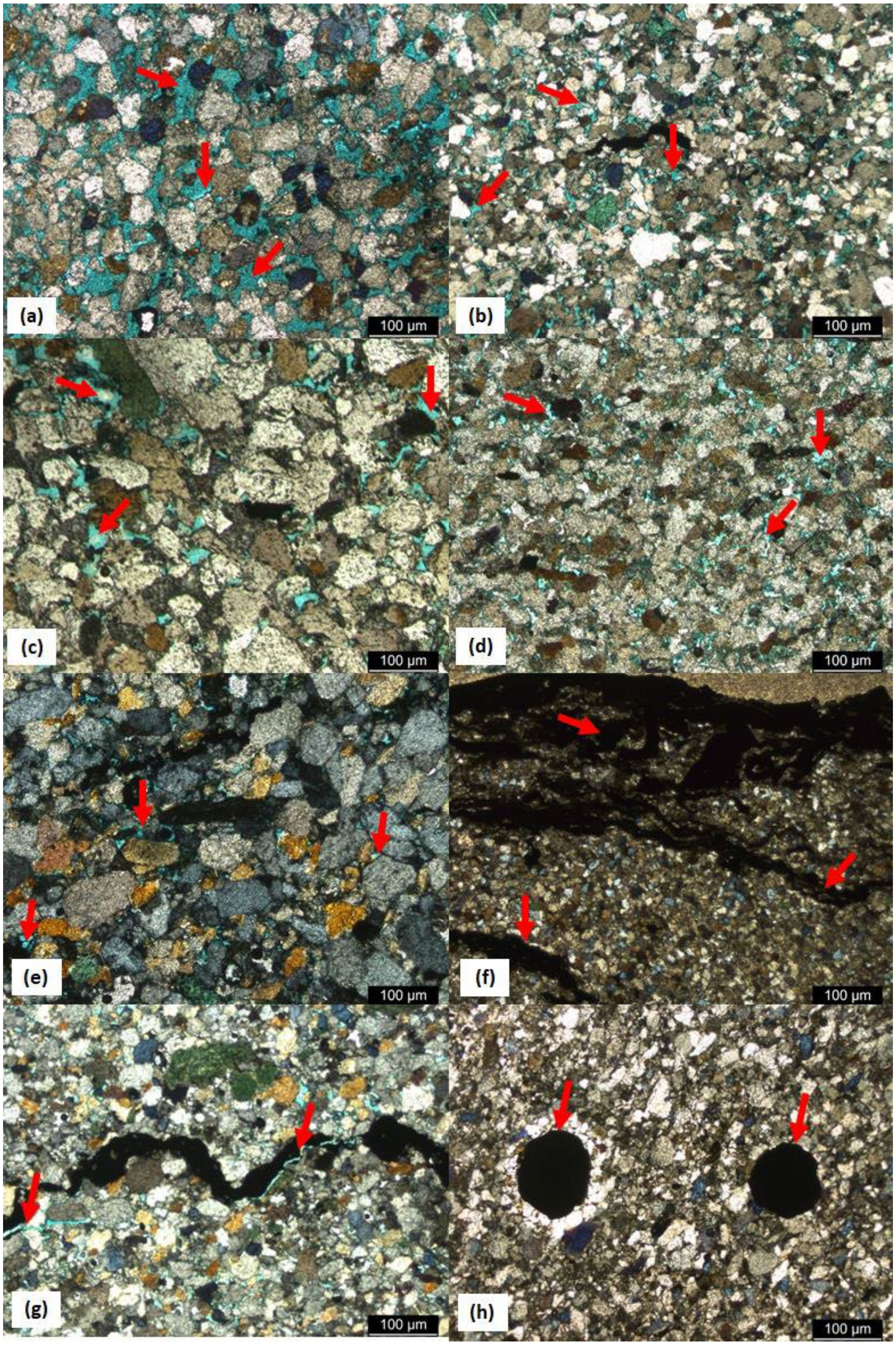

Figure 7. Thin section photomicrograph of sandstone showing some reservoir properties: (a) Primary pore spaces (green areas, red arrows) in Borehole E-AH1 at a depth of 2477 m; (b) pore spaces (green areas, red arrows) in Borehole E-AJ1 at a depth of 2704 m; (c) Pore spaces (green areas, red arrows) in Borehole E-BA1 at a depth of 2835 m; (d) Pore spaces (green areas, red arrows) in Borehole E-BB1 at a depth of 2852 m; (e) Pore spaces (Top: hydrocarbon fills to previously fractured zone, red arrows point to pore space) in Borehole E-D3 at a depth of 3528 m; (f, g) Solid bitumens filling the fractured pores (red arrows) in Borehole E-BB1; (h) Oil emplacement in Borehole E-AJ1

The gas expansion porosity and Klinkenberg corrected permeability are highest in exploration well E-AH1 and lowest in exploration well E-D3, similar to the point count porosity. Sub-arkosic sandstones dominate borehole E-AH1, whereas lithic arkose dominates borehole E-D3. Arkosic sandstones often have higher porosity and permeability percentages. The diversity in their reservoir qualities may have been caused by how these sandstone types responded to diagenetic processes. These variations in porosity and permeability demonstrate the variety of distinct diagenetic processes that affected the sandstones to varying degrees in the various boreholes and under various circumstances. For instance, sandstones with more ductile grains lose permeability when mechanically compacted compared to sandstones with fewer ductile grains. With depth, porosities and permeabilities do not change in any particular order or pattern (Figure 8).

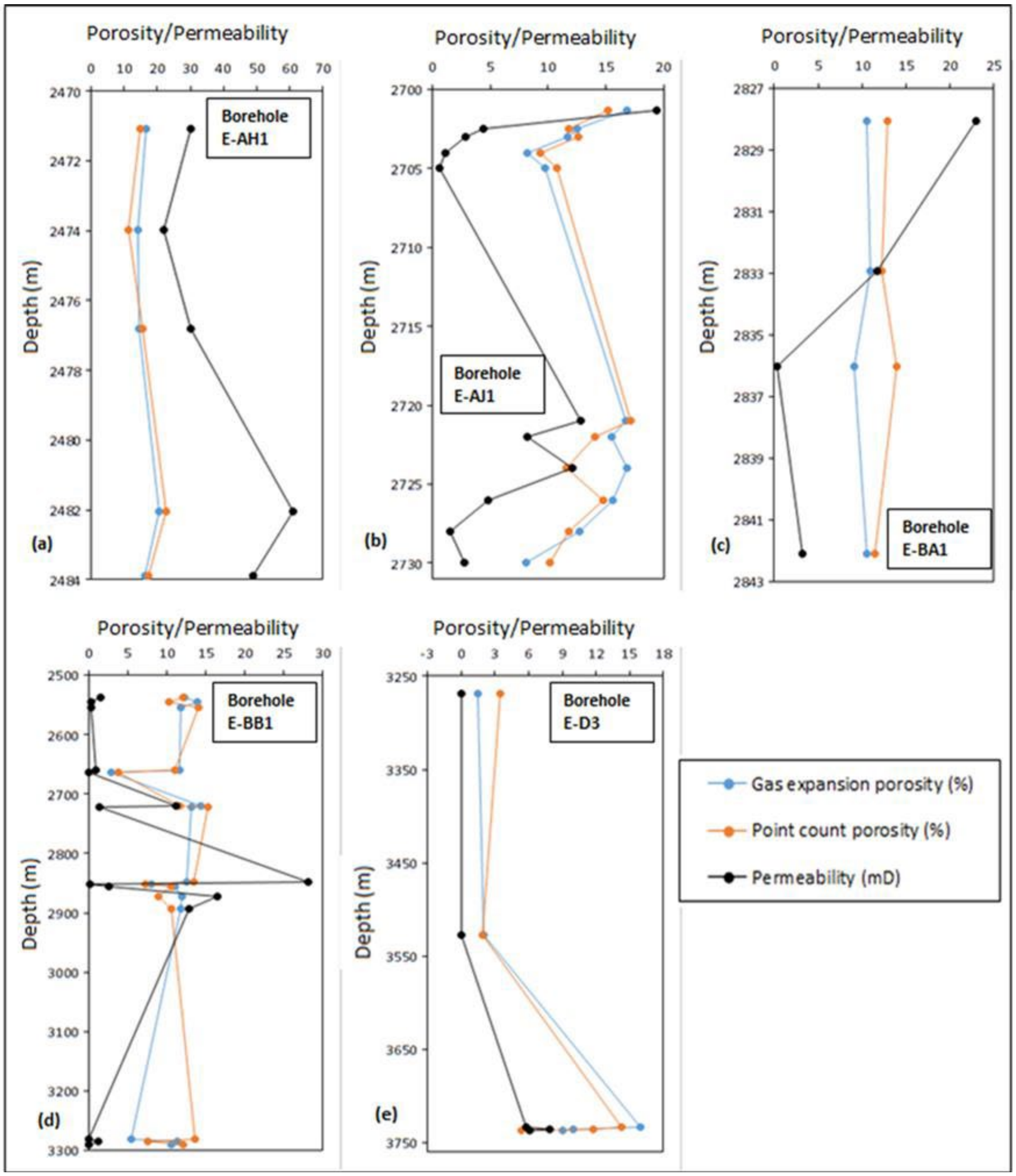

Figure 8. Downhole point count porosity, poroperm porosity and permeability for exploration wells: (a) E-AH1; (b); E-AJ1; (c); E-BA1; (d) E-BB1; (e) E-D3.

Table 3. The summary of the reservoir properties of the sandstones of the southern Bredasdorp Basin

Borehole	Depth (m)	Gas Expansion Porosity (%)	Point Count Porosity (%)	Klinkenberg Corrected Permeability (mD)	Dominant cement under SEM and petrography	Effect of diagenesis on the reservoir properties
E-AH1	2471.08	16.80	14.80	30.00	Quartz, kaolinite, non-ferroan calcite	Porosity and permeability are generally good. Secondary porosities are well developed. The abundance of elongate and oversized pores, and the uncompacted nature of the sandstones suggest that much of the porosity is secondary, after dissolution of an early intergranular cement and detrital grains.
	2473.98	14.20	11.40	22.00		
	2476.80	14.50	15.60	30.00		
	2482.04	20.60	22.70	61.00		
	2483.90	16.30	17.40	49.00		
E-AJ1	2701.30	16.80	15.20	19.40	Quartz and ferroan calcite	Porosity is good and permeability is moderate to good. Quartz commonly fills the secondary pores and the pseudomatrix in some places results in the reduced permeability
	2702.50	12.50	11.80	4.40		
	2703.00	11.70	12.60	2.90	Quartz, ferroan calcite, kaolinite and illite	Porosity is good and permeability is poor to moderate. Secondary porosity is patchy developed, after dissolution of calcite cement. The increase in abundance of fibrous illite, and resultant microporosity development is primarily responsible for poor permeability.
	2704.00	8.20	9.40	1.10		
	2705.00	9.80	10.80	0.60		
	2721.00	16.70	17.20	12.80	Non-ferroan calcite, illite and kaolinite	Porosity and permeability are good. Secondary porosity are well developed, but permeabilities are restricted by fibrous authigenic illite, quartz overgrowths and, to a lesser extent, calcite.
	2722.00	15.50	14.10	8.20		
	2724.00	16.80	11.60	12.10		
	2726.00	15.60	14.80	4.80	Non-ferroan calcite, illite and kaolinite	Porosity is good and permeability is poor to moderate. Fibrous illite, from grain alteration, has reduced the secondary porosity to microporosity in places, resulting in reduced permeability.
	2728.00	12.70	11.80	1.60		
	2730.00	8.10	10.20	2.80		
E-BA1	2828.05	10.50	12.90	43.00	Quartz, kaolinite and calcite	Porosity is good and permeability is moderate to good. Quartz commonly fills the secondary porosity and the pseudomatrix results in it having poorer permeability
	2832.92	11.00	12.30	11.70		
	2836.01	9.10	13.90	0.33	Quartz and kaolinite	Porosity is moderate with poor permeability. Quartz overgrowths and pseudomatrix are the most abundant pore filling phases with lesser kaolinite. Microporosity through pseudomatrix and authigenic clays restricts permeability.
	2842.10	10.50	11.40	3.21		
E-BB1	2538.05	12.30	12.10	1.50	Quartz overgrowth and non-ferroan calcite	Good porosity and poor permeability. Secondary porosity is good and developed by leaching of calcite cement. Porosity is substantially reduced by quartz overgrowths and compaction of claystone clasts to form pseudomatrix. Permeability is restricted by quartz overgrowths and the development of fibrous authigenic illite, creating microporosity.
	2546.00	13.90	10.30	0.30		
	2554.40	11.70	14.10	0.28		
	2659.05	11.60	11.00	0.93		
	2663.18	2.80	3.70	0.01	Quartz and non-ferroan calcite	Poor porosity and permeability. Porosity is reduced by pore filling quartz, quartz overgrowths, calcite and illite are the factors resulting in the poor permeability.
	2720.55	14.30	11.60	11.20	Quartz, illite and kaolinite	Porosity is good and permeability is poor to good. Quartz overgrowths reduce intergranular porosity. Illite also restricts permeability by creating microporosity.
	2722.55	13.20	15.30	1.30		
	2849.05	12.60	13.50	28.10	Quartz overgrowth, illite and kaolinite	Porosity and permeability are generally good.
	2852.03	8.00	7.20	0.09		Porosity is good and permeability is poor. The increase in the amounts of illite and kaolinite and the presence of pseudomatrix accounts for the poor permeabilities.
	2856.05	11.00	10.60	2.60		
	2872.05	11.90	8.90	16.50	Quartz, ferroan calcite and pyrite	Porosity and permeability are generally good. Quartz and calcite commonly fills the secondary porosity and the pseudomatrix in some places results in it having these porosity and permeability
	2894.05	11.70	10.60	12.80		
	3280.06	5.40	13.60	0.01	Ferroan calcite, quartz and illite	Porosity is moderate to good and permeability is generally poor. The reduction in the porosity is due to cementation by calcite, quartz and illite. The permeability is restricted by microporous illite and by quartz overgrowth cementation.
	3284.87	11.30	7.50	1.20		
	3290.31	10.60	12.10	0.02		
E-D3	3268.58	1.50	3.50	0.00	Kaolinite, illite, non-ferroan calcite and quartz overgrowth	Porosity and permeability are very poor. Intergranular porosity is reduced by quartz overgrowths and non-ferroan calcite. Kaolinite, calcite and illite are abundant, producing microporosity, and hence reducing porosity permeability.
	3527.50	2.00	1.90	0.00		
	3733.25	16.00	14.30	5.80	Quartz overgrowth, non-ferroan calcite and pyrite	Porosity and permeability are good. Quartz overgrowths and calcite have reduced intergranular porosity. Secondary porosity is developed by leaching of calcite cement, but is commonly reduced to microporosity by authigenic illite.
	3736.03	10.00	11.80	7.90		
	3737.00	9.00	5.40	6.10		

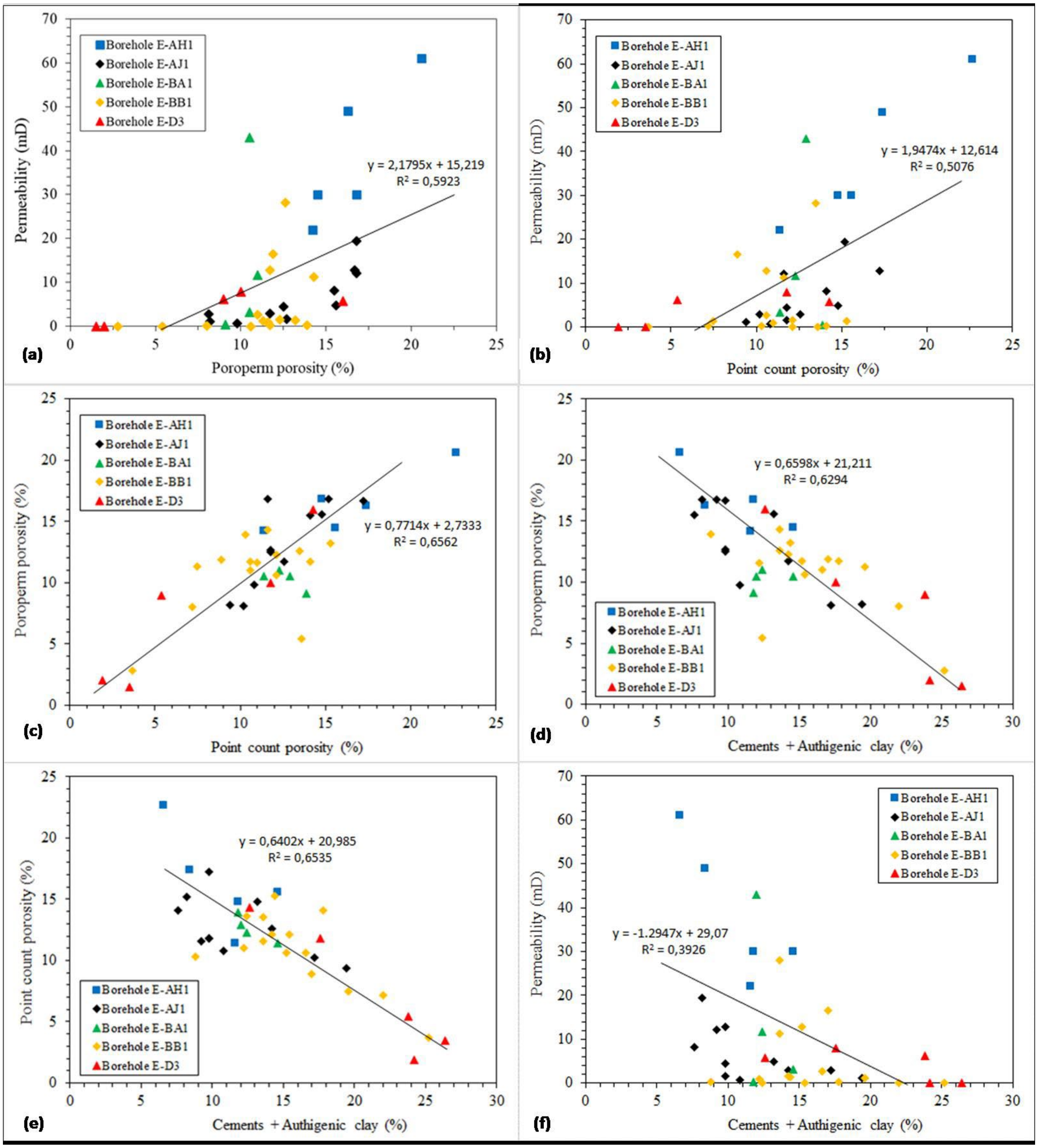

Figure 9. Scatter plots of the reservoir property data of the Bredasdorp Basin sandstones showing the relationship between visual point counted porosity, gas expansion porosity, permeability, and cements plus authigenic clays: (a) Gas expansion porosity versus permeability; (b) Point counted porosity against permeability; (c) Point counted porosity versus gas expansion porosity; (d) Cements + authigenic clays against gas expansion porosity; (e) Cements + authigenic clays versus point counted porosity; (f) Cements + authigenic clays against permeability

The cementation of clay minerals is the primary diagenetic process that has had a substantial impact on the reservoir qualities of the sandstones. Each borehole, at varying depths, and with varied sand units responded differently to the various controls (such as detrital matrix and cements) on reservoir quality. When compared to deeper buried sand units, sandstones at shallow depths should be more permeable. The majority of the investigated boreholes, however, exhibit the contrary. For instance, in boreholes E-D3, the porosity of the sand unit varies between 2-3.5% at a depth of about 3268 m but drops to 1.5-2% at a depth of about 3527 m, possibly indicating the influence of compaction due to increased overburden or burial depth. Contrarily, this porosity, which was 1.5-2% at a depth of about 3527 m, increased to 12.5-15 % at a depth of about 3733 m, and then abruptly decreased to 3-4% at a depth of about 3740 m. Petrographic and SEM observations of the sandstones from the depths of 3733–3740 m show that secondary porosity is developed in the sandstones by the leaching of calcite cement and dissolution of feldspar. However, at a depth of roughly 3740 m, authigenic illite reduces this porosity to microporosity. The influence of compaction and cementation is complex and lacks any discernible pattern in boreholes E-AJ1 and E-BB1, which may indicate that diagenesis is the principal obstacle to reservoir characterization in the Bredasdorp Basin. Facies variation with depth in the boreholes, as well as the depositional environment (i.e., distal and proximal areas), could have influenced the reservoir properties of the individual boreholes. However, in this study, proximal and distal areas, reworking, and facies variations were not interpreted or evaluated.

In no particular order with increasing burial depth, the percentage of detrital matrix and cement in boreholes E-AH1, E-AJ1, E-BA1, E-BB1 and E-D3 varies between 8.8–20.2%, 8.6–15.2%, 7.6–16%, 10.4–20.6% and 12.4–16.8%, respectively. This could imply that diagenesis is the primary determinant of reservoir properties. Although both primary and secondary pore types are present at various depth intervals in the sandstones, the extensive matrix in some of the sandstones impedes cementation by inhibiting the nucleation of overgrowths. Petrographic and scanning electron microscopy (SEM) examinations of the sandstones revealed that areas (depths) with fewer clay minerals are frequently associated with high porosity and permeability, and vice versa. Areas with high permeability values typically have significant primary porosity preservation and/or extensive secondary porosity development. In samples where large, isolated secondary pores form as a result of grain and/or cement dissolution, they frequently have high porosity and slightly lower permeability.

The petrographic studies revealed a number of diagenetic controls on porosity development, including cementation and compaction. It also shows that porosity increases in samples of floating to point contacts and decreases in samples of long, concave-convex, and sutured contacts (Figure 7). A scatter plot of point counted porosity and gas expansion porosity against permeability reveals a positive correlation (Figure 9a-c). Furthermore, the binary plot of point count porosity versus gas expansion porosity has a direct or positive correlation, indicating that the porosity values are reliable. The main cements that influence the reservoir properties of sandstones are silica, carbonate, and authigenic clay cements. To statistically investigate these controls on porosity, the sum of cements and authigenic clays were plotted against point counted porosity, gas expansion porosity, and permeability, and they all have a relatively good inverse correlation (Figure 9d-f). This negative or inverse correlation indicates that these controls are the most important ones to consider when predicting reservoir quality. Carbonate cement, particularly poikilitopic calcite, tends to assemble in pores, obstructing pore throats. As a result, it reduces permeability more than grain coating cements such as quartz overgrowth.

5.4. Diagenetic sequence

Based on the overall correlations of the recognized diagenetic processes, a paragenetic sequence has been created for the Bredasdorp Basin sandstones (Table 4). SEM+EDX, XRD, and petrographic examinations were used to derive this paragenetic sequence, which depicts all diagenetic events in relation to their relative period of formation. The paragenetic sequence revealed that the sandstones underwent intense and complex diagenesis episodes during the early, middle, and late diagenetic stages. In the early diagenetic stage, the main diagenetic events are detrital clay infiltration, pyrite formation, glauconitization, carbonate cements, authigenic clays, early dissolution of unstable clastic grains (i.e., feldspar and rock fragments), and minor mechanical compaction. Mechanical compaction, recrystallization, replacement, pressure solution, and mineral dissolution are the main diagenetic events during the burial stage. Dissolution (decementation), grain fracturing, and the development of stylolites characterize the late diagenetic stage.

Table 4. Paragenetic sequence of the Bredasdorp Basin sandstones as established in this study

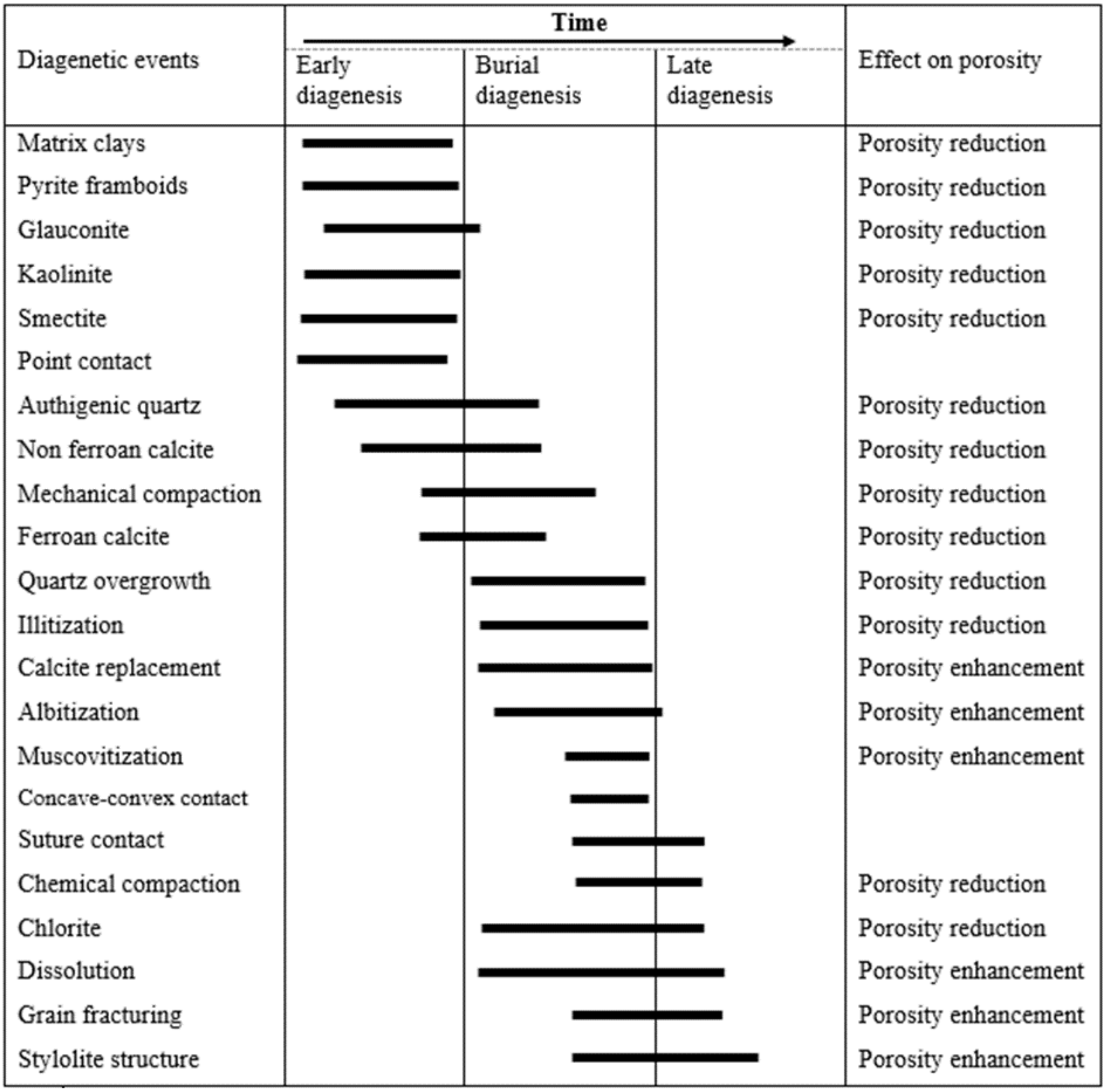

5.5. Implications of diagenesis for reservoir quality

The Bredasdorp Basin's diagenetic environment was constantly changing, resulting in the complex diagenetic phenomena seen in the current reservoirs. Diagenesis alters the original pore type and geometry of sandstones, thereby controlling their final porosity and permeability. When predicting the reservoir quality of sandstones, it is critical to have a good understanding or interpretation of the diagenetic history as a product of depositional environments, sediment composition, and fluid migration patterns [34,48]. The reservoir quality of the Bredasdorp Basin sandstones is primarily controlled by diagenetic processes that reduce or increase porosity and permeability. The most important diagenetic processes that affected the reservoir quality of the sandstones were mechanical compaction, cementation by carbonate (calcite), glauconite, silica (quartz), sulphide (pyrite), and authigenic clay (kaolinite, illite, smectite, and chlorite), and mineral dissolution (i.e., feldspar). Because of progressive burial, grain contact changes from point contacts to sutured contacts as the deposited sands become compacted, resulting in a reduction in primary intergranular porosity and pore radii.

Primary porosities are the most abundant, but they are reduced by calcite cementation, the formation of authigenic clays, and compaction. Kaolinite is the most abundant authigenic clay in the studied sandstones, appearing as rims around detrital grains as well as pore-lining and pore-filling cements. This clay acts as a pore-choking cement, reducing porosity and creating a permeability barrier while also potentially presenting irreducible water saturation traps. While kaolinite infilling pores appears to reduce porosity, it retains a significant amount of microporosity. The main problem with kaolinite is that the individual plates are prone to being removed during oil production and blocking the pore-throats, resulting in a significant reduction in permeability [49]. Also, the amount of fibrous illite in the studied sandstones is small, so its effect on sandstone permeability is negligible. Kaolinite and mixed layer clays reduce primary porosity while also forming and preserving microporosity within kaolinite crystals. The early formed non-ferroan calcite cement fills in primary porosity and occludes pore throat, whereas the ferroan calcite cements fill in residual primary porosity as well as secondary porosity created by feldspar dissolution [34]. Silica cements frequently destroy primary porosity, and their presence in sandstones may impede primary porosity preservation. Quartz overgrowths in the sandstones coat the detrital quartz grains and reduce pore radii, resulting in decreased porosity and permeability. Pyrite cement is present in minor amounts but, to some extent, restricts pore geometry and pore size distribution locally.

Secondary intragranular pores, dissolution pores, and fractured pores were observed in the sandstones. Secondary intragranular and dissolution pores are formed as a result of detrital feldspar grain dissolution, clay mineral dissolution caused by pseudomatrix alteration, and carbonate cement dissolution. The fractured pores are also caused by structural forces and differential compaction. These secondary porosities caused by feldspar and carbonate cement dissolution has improved the reservoir quality of the sandstones to varying degrees. In general, pseudomatrix and silica cements reduce sandstone porosities significantly. The formation of fibrous authigenic illite, quartz overgrowths, and, to a lesser extent, carbonate and pyrite cements has hampered permeability. The majority of the samples with low porosity and permeability values underwent pressure solution along carbonaceous streaks, resulting in more extensive quartz and kaolinite cementation. Deeper samples with low porosity also exhibit pervasive silica cements and the formation of pseudomatrix. As a result, secondary porosity development is very low or non-existent. Diagenesis has considerably reduced the reservoir quality of the Bredasdorp Basin sandstones, despite the formation of secondary porosity. The impact of diagenesis on reservoir quality varies depending on borehole, depth, and sand unit. Furthermore, the intermittent introduction of increased and decreased temperatures, followed by decreased temperatures, has influenced diagenesis of the basin [50].

6. Conclusions

The sandstones of the Bredasdorp Basin are predominantly fine-grained and moderately well-sorted, and they could be classified as subarkose. The modal composition analysis (QFL ternary diagrams) indicates that the sandstones are largely derived from granites and granite–gneisses of a continental block tectonic setting (craton interior and transitional continental) in a rifted continental margin basin setting, suggesting that the sandstones were derived from stable shields and uplifted areas. The tectonic setting discrimination diagrams support the passive-active continental margin setting of the provenance. In addition, the closely similar geochemical compositions of the analysed samples and those of recent sedimentary rocks of the East African Rift System perhaps suggest a rifted basin tectonic setting for the Bredasdorp Basin. The sandstones exhibit good reservoir characteristics in some intervals due to high porosity and permeability, but poor reservoir characteristics in others due to low porosity and permeability. The high reservoir quality in boreholes E-AH1 and E-D3 is the result of diagenetic processes (such as dissolution, leaching, and grain fracturing) that increased porosity and permeability. In contrast, the poor reservoir quality in borehole E-D3 is caused by authigenic clay cementation and compaction (i.e., concavo-convex and suture contacts). The various reservoir quality controls operate differently in each borehole and at different depths and sand units. The effect of cementation and compaction is complex, with no discernible pattern as depth increases, implying that diagenesis is the primary challenge to reservoir characterization in the Bredasdorp Basin. In general, no single diagenetic process is solely responsible for the type or form of porosity evolution in sandstones. Instead, it appears that the main types of cement (clay minerals, calcite, and silica) and, to a lesser extent, compaction collectively controlled the sandstone reservoir quality.

Acknowledgments

The authors are grateful to the Petroleum Agency of South Africa (PASA) and the Govan Mbeki Research and Development Centre (GMRDC) of the University of Fort Hare are appreciated for granting acces to the cores and logistic supports, respectively.

References

[1] Burden PLA. Soekor, partners explore possibilities in Bredasdorp Basin off South Africa. Oil and Gas Journal, 1992; 90 (51): 109–112.
[2] Zou C, Zhu R, Liu K, Su L, Bai B, Zhang X, Yuan X, and Wang J. Tight gas sandstone reservoirs in China: Characteristics and recognition criteria. Journal of Petroleum Science and Engineering, 2012; 88: 82–91.
[3] Baiyegunhi C, Liu K, and Gwavava O. Grain size statistics and depositional pattern of the Ecca Group sandstones, Karoo Supergroup in the Eastern Cape Province, South Africa. Open Geosciences, 2017a; 9: 554–576.
[4] Akinlua A, Sigedle A, Buthelezi T, and Fadipe OA. Trace element geochemistry of crude oils and condensates from South African Basins. Marine and Petroleum Geology, 2015; 59: 286–293.
[5] Taylor RT, Giles MR, Hathon LA, Diggs TN, Braunsdorf NR, Birbiglia GV, Kittridge MG, Macaulay CI, and Espejo IS. Sandstone diagenesis and reservoir quality prediction: Models, myths, and reality. AAPG Bulletin, 2010; 94: 1093–1132.
[6] Bloch S, Lander RH, and Bonell L. Anomalously high porosity and permeability in deeply buried sandstones reservoirs. Origin and predictability. AAPG Bulletin, 2002; 86: 301–328.
[7] Burley SD, and Worden RH. Sandstone diagenesis: The evolution of sand to stone, in S.D. Burley and R.H. Worden (Eds.), Sandstone Diagenesis; Recent and Ancient: Blackwell Publishing, Malden, MA, International Association of Sedimentologists Reprint Series, 2003; 4: 34–44.
[8] Macquaker JHS, Taylor KG, Keller M, and Polya D. Compositional controls on early diagenetic pathways in fine-grained sedimentary rocks: Implications for predicting unconventional reservoir attributes of mudstones. American Association of Petroleum Geologists (AAPG Bulletin),2014; 93: 587–603.
[9] Ajdukiewicz JM and Lander RH. Sandstone reservoir quality prediction: the state of the art. AAPG Bulletin, 2010; 94 (8): 1083–1091.
[10] Boggs S Jr. Petrology of Sedimentary Rocks, Second Edition. Cambridge University Press, UK, 2009; 600p.
[11] Roswell DM, and De Swart AMJ. Diagenesis in Cape and Karroo sediments, South Africa, and its bearing on their hydrocarbon potential. Transactions of the Geology Society of South Africa, 1976; 79: 81–145.
[12] Reed JS, Eriksson KA, and Kowalewski M. Climatic, depositional and burial controls on diagenesis of Appalachian Carboniferous sandstones: qualitative and quantitative methods. Sedimentary Geology, 2005; 176: 225–246.
[13] Chima P, Baiyegunhi C, Liu K, and Gwavava O. Diagenesis and rock properties of sandstones from the Stormberg Group, Karoo Supergroup in the Eastern Cape Province of South Africa. Open Geosciences, 2018a; 10: 740–771.
[14] Taylor SR, and McLennan SM. The Continental Crust: Its Composition and Evolution. Blackwell Scientific Publications, 1985; 275–293.
[15] Bhatia MR, and Crook KAW. Trace element characteristics of greywacke and tectonic setting discrimination of sedimentary basins. Contributions to Mineralogy and Petrology, 1986; 92: 181–193.
[16] Pettijohn FJ, Potter PE, and Siever R. Sand and Sandstone. Springer, New York,1987; 553p.
[17] Bhatia MR. Plate tectonics and geochemical composition of sandstones. Journal of Geology, 1983; 91: 611–627.

[18] Armstrong-Altrin JS, and Verma SP. Critical evaluation of six tectonic setting discrimination diagrams using geochemical data of Neohene sediments from known tectonic settings. Sedimentary Geology 2005; 177 (1-2): 115–129.
[19] Suttner LJ, Basu A, Mack, GM. Climate and the origin of quartzarenites. Journal of Sedimentary Petrology, 1981; 51:1235–1246.
[20] Dickinson WR., Beard LS, Brakenridge G R, Erjavec JL, Ferguson RG, Inman KF, Knepp, RA, Lindberg FA. and Ryberg PT. Provenance of North Phanerozoic sandstones in relation to tectonic setting. Geol. Soc. Am. Bull. 1983; 94: 222–235.
[21] Weltje GJ, Meijer XD, De Boer PL. Stratigraphic inversion of siliciclastic basin fills: a note on the distinction between supply signals resulting from tectonic and climatic forcing. Basin Research 1998; 10: 129–153.
[22] Suttner LJ, and Dutta PK. Alluvial sandstone composition and palaeoclimate: I. Framework mineralogy. Journal of Sedimentary Petrology, 1986; 56: 329–345.
[23] Roser BP, and Korsch RJ. Determination of tectonic setting of sandstone-mudstone suites using SiO_2 content and K_2O/Na_2O ratio. Journal of Geology, 1986; 94: 635–650.
[24] Roser BP, and Korsch RJ. Provenance signature of sandstone mudstone suite determined using discriminant function analysis of major element data: Chemical Geology, 1988; 67: 119–139.
[25] Armstrong-Altrin JS, Lee YI, Verma SP, and Ramasamy S. Geochemistry of sandstones from the Upper Miocene Kudankulam Formation, southern India: implication for provenance, weathering and tectonic setting: Journal of Sedimentary Research, 2004; 74: 285–297.
[26] Sonibare WA. Structure and evolution of basin and petroleum systems within a transform-related passive margin setting: data-based insights from crust-scale 3D modelling of the Western Bredasdorp Basin, offshore South Africa. PhD. Thesis, University of Stellenbosch, 2015; 294p.
[27] Brown LF, Benson JM, Brink GJ, Doherty S, Jollands A, Jungslager EHA, Keenan JHG, Muntingh A, and Van Wyk NJS. Sequence stratigraphy in offshore South African divergent basins. In: Am. Ass. Petrol. Geol., Studies in Geology, 41, An Atlas on Exploration for Cretaceous Lowstand traps, by Soeker (Pty) Ltd, 1995; 83–131.
[28] Jungslager EHA. Geological evaluation of the remaining prospectivity for oil and gas of the Pre-1At1 "Synrift" succession in Block 9, Republic of South Africa. Unpublished Soekor Technical Report SOE-EXP-RPT-0380, 1996; 63p.
[29] McMillan IK, Brink GJ, Broad DS, and Maier JJ. Late Mesozoic sedimentary basins off the south coast of South Africa, in Selley, R.C., ed., Sedimentary basins of the world—African basins: Amsterdam, Elsevier Science B.V.,1997; 319–376.
[30] Petroleum Agency South Africa PASA. Western Bredasdorp Basin: Petroleum Agency South Africa brochure, 2009; 13–16.
[31] Petroleum Agency South Africa PASA. Petroleum exploration in South Africa, information and opportunities. Online Report, Cape Town, 2012; 25–29. http://www.petroleumagencysa.com/images/pdfs/pet_expl_opp_2012fw.pdf
[32] Broad DS, Jungslager EHA, McLachlan IR, and Roux J. Offshore Mesozoic Basins. In: Johnson, MR, Anhaeusser CR, and Thomas RJ. (Eds.). The Geology of South Africa. Geological Society of South Africa, Johannesburg/Council for Geoscience, Pretoria, 2006; 553–571.
[33] Tinker J, de Wit M, and Brown R. Linking source and sink: evaluating the balance between onshore erosion and offshore sediment accumulation since Gondwana break-up, south Africa. Tectonophysics, 2008; 455(1): 94–103.
[34] Burden PLA, and Davies CPN. Exploration to first production on block 9 off South Africa: Oil and Gas Journal, 1997; 1: 92–98.
[35] Dickinson WR and Suczek C. Plate tectonics and sandstone composition. Am. Assoc. Pet. Geol. Bull. 1979; 63, 2164–2194.
[36] Rietveld HM. The Rietveld method. Physica Scripta, 2014; 89(9): 1–9.
[37] Dott RH. Wackes, greywacke and matrix: what approach to immature sandstone classification. Journal of Sedimentary Petrology, 1964; 34: 625–632.
[38] Folk RL. Petrology of Sedimentary Rock (second ed.,), Hemphill Press, Austin, Texas, 1974; 182p.
[39] Herron MM. Geochemical classification of terrigenous sands and shales from core or log data. Journal of Sedimentary Petrology, 1988; 58; 820–829.
[40] Banerjee A, and Banerjee DM. Modal analysis and geochemistry of two sandstones of the Bhander Group (Late Neoproterozoic) in parts of the Central India, Vindhyan basin and their bearing on the provenance and tectonics. J. Earth Syst. Sci. 2010; 119: 825–839.

[41] Oghenekome ME, Chatterjee TK, Hammond NQ, and van Bever Donker JM. Provenance study from petrography of the late Permian e Early Triassic sandstones of the Balfour Formation Karoo Supergroup, South Africa. Journal of African Earth Sciences, 2016; 114: 125–132.
[42] Baiyegunhi C, Liu K, and Gwavava O. Modal composition and tectonic provenance of the sandstones of Ecca Group, Karoo Supergroup in the Eastern Cape Province, South Africa. Open Geosciences, 2017b; 9: 491–508.
[43] Chima P, Baiyegunhi C, Liu K, and Gwavava O. Petrography, modal composition and tectonic provenance of some selected sandstones from the Stormberg Group, Karoo Supergroup, in the Eastern Cape Province, South Africa. Open Geosciences, 2018b; 10: 821–833.
[44] Yerino LN, and Maynard JB. Petrography of modern marine sands from the Peru-Chile Trench and adjacent areas. Sedimentology, 1984; 31: 83–89.
[45] Dickinson WR. Provenance and Sediment Dispersal in Relation to Paleotectonics and Paleogeography of Sedimentary Basins. In: Kleinspehn, K.L., Poala, C. (Eds.), New Perspectives in Basin Analysis. Springer-Verlag, New York, 1988; 2–25.
[46] Kumon F, Kiminami K, Adachi M, Bessho T, Kusunoki T, Mishimura T, Okada H, Okami K, Suzuki S, and Teraoka Y. Modal compositions of representative sandstones from the Japanese Islands and their tectonic implications. Mem. Geol. Soc. Japan, 1992; 38: 385–400.
[47] McLennan SM, Hemming S, McDaniel DK, and Hanson GN. Geochemical approaches to sedimentation, provenance and tectonics, in: Johnsson, M.J. and Basu, A. (Eds.), Processes Controlling the Composition of Clastic Sediments. Geological Society of American Special Paper, 1993; 21–40.
[48] Acho BC. Assessing hydrocarbon potential in Cretaceous sediments in the western Bredasdorp sub-basin in the Outeniqua Basin South Africa. MSc dissertation (Unpublished), University of Western Cape, 2015; 197p.
[49] Broad DS, and Mills SR. South Africa offshore exploratory potential in variety of basins. Oil and Gas Journal, 1993; 91: 38–44.
[50] Hartnady CJH. and Le Roex AP. Southern Ocean hotspot tracks and the Cenozoic absolute motion of the African, Antarctic and South American plates. Earth Planetary Science Letters, 1985; 75: 245–257.

To whom correspondence should be addressed: Dr. Temitope Love Baiyegunhi, Department of Geology, Faculty of Science and Agriculture, University of Fort Hare, Private Bag X1314, Alice, 5700, Eastern Cape Province, South Africa, E-mail: 201814648@ufh.ac.za; lovetemitope18@gmail.com